PARP-1 Activation Directs FUS to DNA Damage Sites to Form PARG-Reversible Compartments Enriched in Damaged DNA

Anastasia Singatulina, Loic Hamon, Maria Sukhanova, Bénédicte Desforges, Vandana Joshi, Ahmed Bouhss, Olga Lavrik, David Pastre

Article

Cell Reports

PARP-1 Activation Directs FUS to DNA Damage Sites to Form PARG-Reversible Compartments Enriched in Damaged DNA

Graphical Abstract

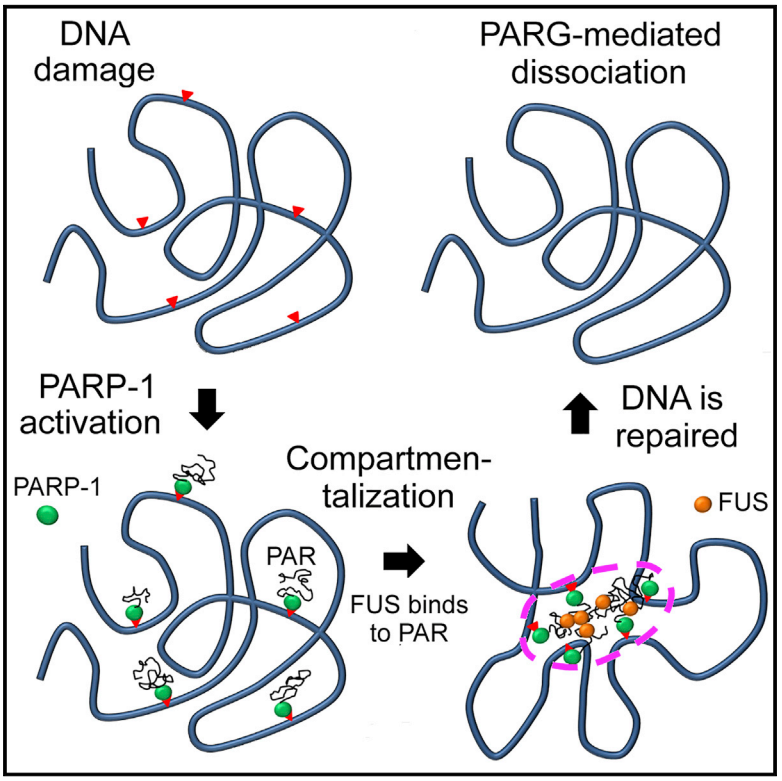

Authors

Anastasia S. Singatulina, Loic Hamon, Maria V. Sukhanova, ..., Ahmed Bouhss, Olga I. Lavrik, David Pastré

Correspondence

lavrik@niboch.nsc.ru (O.I.L.), david.pastre@univ-evry.fr (D.P.)

In Brief

Using a single-molecule approach, Singatulina et al. reconstitute the DNA repair system leading to the specific recruitment of FUS, an mRNA-binding protein related to liquid-liquid phase separation biology, to DNA damage sites, thus revealing the capacity of FUS to form dynamic compartments in which damaged DNA is concentrated.

Highlights

- FUS is directed to DNA damage sites by binding PAR synthesized by PARP-1
- FUS then forms large compartments in which damaged DNA is concentrated
- PARG dissociates damaged DNA compartments by hydrolyzing PAR
- Then FUS shuttles from the nucleus to the cytoplasm

Singatulina et al., 2019, Cell Reports *27*, 1809–1821
May 7, 2019
https://doi.org/10.1016/j.celrep.2019.04.031

CellPress

Cell Reports
Article

PARP-1 Activation Directs FUS to DNA Damage Sites to Form PARG-Reversible Compartments Enriched in Damaged DNA

Anastasia S. Singatulina,[1,2] Loic Hamon,[1] Maria V. Sukhanova,[2] Bénédicte Desforges,[1] Vandana Joshi,[1] Ahmed Bouhss,[1] Olga I. Lavrik,[2,3,*] and David Pastré[1,4,*]
[1]SABNP, Univ Evry, INSERM U1204, Université Paris-Saclay, 91025 Evry, France
[2]Institute of Chemical Biology and Fundamental Medicine, Novosibirsk 630090, Russia
[3]Department of Natural Sciences, Novosibirsk State University, Novosibirsk 630090, Russia
[4]Lead Contact
*Correspondence: lavrik@niboch.nsc.ru (O.I.L.), david.pastre@univ-evry.fr (D.P.)
https://doi.org/10.1016/j.celrep.2019.04.031

SUMMARY

PARP-1 synthesizes long poly(ADP-ribose) chains (PAR) at DNA damage sites to recruit DNA repair factors. Among proteins relocated on damaged DNA, the RNA-binding protein FUS is one of the most abundant, raising the issue about its involvement in DNA repair. Here, we reconstituted the PARP-1/PAR/DNA system *in vitro* and analyzed at the single-molecule level the role of FUS. We demonstrate successively the dissociation of FUS from mRNA, its recruitment at DNA damage sites through its binding to PAR, and the assembly of damaged DNA-rich compartments. PARG, an enzyme family that hydrolyzes PAR, is sufficient to dissociate damaged DNA-rich compartments *in vitro* and initiates the nucleocytoplasmic shuttling of FUS in cells. We anticipate that, consistent with previous models, FUS facilitates DNA repair through the transient compartmentalization of DNA damage sites. The nucleocytoplasmic shuttling of FUS after the PARG-mediated compartment dissociation may participate in the formation of cytoplasmic FUS aggregates.

INTRODUCTION

In mammalian cells, DNA single- and double-strand breaks (SSBs and DSBs, respectively) (Ciccia and Elledge, 2010; Schreiber et al., 2006) trigger a complex cascade of events in which the members of the ADP-ribosyltransferase family—PARP-1 being the most abundant—recognize DNA damage sites and synthesize long and branched poly(ADP-ribose) (PAR) chains covalently attached to themselves or to other acceptor proteins. PAR is hydrolyzed by poly(ADP-ribose) glycohydrolase (PARG) (Illuzzi et al., 2014), which makes PARylation of acceptor proteins a reversible post-translational modification. Both high PARylation level among RNA-binding proteins (RBPs) (Gagné et al., 2012; Jungmichel et al., 2013) and their abundance in nuclear regions damaged by short laser beam exposures (Izhar et al., 2015; Rulten et al., 2014) raise issues about the putative role of RBPs in DNA damage response (Bock et al., 2015; Leung, 2014). Here, we focus our attention on FUS (FUS/TLS, Fused in Sarcoma) and its mutant forms. FUS, together with EWS and TAF15, is a member of the FET family and one of the most abundant and highly PARylated nuclear RNA-binding proteins (Britton et al., 2014; Singh et al., 2015; Zhen et al., 2017).

As shown in previous studies, multivalent interactions occurring between the low-complexity domains (LCDs) of RNA-binding proteins (Banani et al., 2017) such as FUS, TDP-43, and TIA-1 participate in the formation of membraneless compartments (Bergeron-Sandoval et al., 2016; Li et al., 2012; Patel et al., 2015; Zhang et al., 2015), among them being stress granules (Strzyz, 2016), nucleoli (Feric et al., 2016), nuclear speckles (Zhu and Brangwynne, 2015), and paraspeckles (Hennig et al., 2015). FUS has been intensively studied because of its link to neurodegenerative diseases and cancer (Aguzzi and Altmeyer, 2016). In addition, FUS condensates have liquid-like properties whose dynamics and structure are affected by pathogenic mutations (Patel et al., 2015) and controlled by phosphorylation of its N-terminal LCD (Monahan et al., 2017; Murray et al., 2017). It was proposed that the C-terminal RGG repeats of FUS also participate in liquid-liquid phase separation and that arginine methylation may modulate the properties of FUS condensates (Hofweber et al., 2018; Qamar et al., 2018).

The interplay between FUS and PAR has been examined since the recruitment of FUS to DNA damaged regions was evidenced (Altmeyer et al., 2015; Mastrocola et al., 2013; Naumann et al., 2018; Patel et al., 2015; Rulten et al., 2014). *In vitro* analyses also demonstrated that purified PAR interacts directly with FUS to promote liquid-liquid phase separation (Altmeyer et al., 2015; Patel et al., 2015; Teloni and Altmeyer, 2016), which requires the C-terminal positively charged RGG domains (Altmeyer et al., 2015). As RGG domains are also involved in the binding of FUS to mRNA, mRNA and PAR may, therefore, compete for the electrostatic binding to FUS (Altmeyer et al., 2015).

The formation of FUS-rich compartments in DNA regions exposed to laser beam is transient, lasting no more than 15–30 min (Altmeyer et al., 2015; Mastrocola et al., 2013; Patel et al., 2015; Rulten et al., 2014). A rapid dissociation of these compartments may be necessary to resume performing normal DNA-related processes. In cells, reducing PAR hydrolysis by silencing PARG delays the dissociation of FUS-rich

compartments in the nucleus (Altmeyer et al., 2015; Naumann et al., 2018; Patel et al., 2015), suggesting that PARG hydrolyzes PAR to release the protein factors that previously were recruited to DNA damage sites. Recently, PARG activity has been also associated with an increased presence of FUS in the cytoplasm of neurons after stress (Naumann et al., 2018). However, phosphorylation of FUS residues in the LCD, notably by DNA-dependent protein kinase (DNA-PK) (Deng et al., 2014; Monahan et al., 2017), and methylation of the RGG domains (Kaneb et al., 2012) may also participate in the nucleocytoplasmic shuttling, even if this is still a debated issue (Rhoads et al., 2018). The PARG-dependent translocation of FUS provides an interesting link between DNA repair and neurodegenerative diseases (Naumann et al., 2018).

While cellular observations suggest that FUS could bind to PAR synthesized at DNA damage sites to form transient liquid-like compartments (Altmeyer et al., 2015; Naumann et al., 2018; Patel et al., 2015; Rulten et al., 2014), many proteins are recruited to DNA damage sites after laser beam exposures. The molecular mechanisms responsible for the formation and the possible functions of these compartments are, therefore, difficult to address in a cellular context. Here, we developed an original approach based on a single molecule analysis by atomic force microscopy (AFM) (Hamon et al., 2007; Sukhanova et al., 2016) to reconstitute the molecular system that serves to recruit FUS at DNA damage sites, including factors such as intact and damaged DNA, PARP-1, and mRNA that have not been previously considered *in vitro*. Through this *in vitro* system, the binding events and the molecular assemblies orchestrated by FUS at DNA damage sites after PARP-1 activation were dissected. We evidenced the local recruitment of FUS to PAR synthesized by PARP-1 at damaged DNA sites. Importantly, we also found that FUS then triggers the formation of large compartments in which damaged DNA is enriched, even in the presence of mRNA. Consistent with the role of kinases, notably DNA-PK, in controlling the formation of FUS liquid-like compartments, the assembly of damaged DNA compartments is progressively impaired by mutations mimicking phosphorylation in FUS LCDs.

Moreover, we demonstrate the reversible nature of these compartments as the hydrolysis of PAR by PARG is sufficient to dissociate damaged-DNA compartments formed by FUS. Consistent with results in neuron cells (Naumann et al., 2018), we show that PARP-1 activation leads to the shuttling of FUS from the nucleus to the cytoplasm in H_2O_2-treated HeLa cells. In addition, we demonstrate that FUS translocation takes place at a later stage (>15 min) when PARG activity promotes the dissociation of damaged-DNA compartments in the nucleus. Other nuclear mRNA-binding proteins (TDP-43 and TIA-1) that also contain RNA-recognition motifs (RRMs) and LCDs with prion-like properties do not follow the same trend.

In light of these results, we anticipate that the transient formation of damaged DNA-rich compartments can promote the rapid repair of damaged DNA that does not rely on homologous recombination. The shuttling of FUS to the cytoplasm after the dissociation of damaged-DNA rich compartments may, in turn, participate in an adapted translational response to DNA damage, but the presence of such an aggregation-prone protein in the cytoplasm may also provide a link between PARP-1 activation and neurodegenerative diseases (Hoch et al., 2017; Li et al., 2013; Naumann et al., 2018).

RESULTS

FUS Leads to the Formation of Large Compartments Containing DNA and PAR

We recently found optimal conditions to visualize the synthesis of PAR polymers after the activation of PARP-1 on DNA damage sites at the single-molecule level by AFM (Sukhanova et al., 2016). Although PAR is known to promote liquid-liquid phase separation of FUS *in vitro* (Patel et al., 2015), no nanoscopic view of PAR:FUS self-assembly or any interplay with DNA and PARP-1 was reported. In addition, we planned to visualize and analyze the interaction of FUS with PAR in the presence of damaged DNA to trigger PAR synthesis by PARP-1 at damaged DNA sites. To undertake this study, a long linear DNA fragment with a single DNA break (1,200-bp nicked DNA) was used to analyze whether PARP-1 activation leads to the synthesis of PAR at damaged DNA sites in the presence of NAD^+ (Figure 1A). While FUS has a weak affinity for double-stranded DNA (dsDNA) (Sama et al., 2014; Wang et al., 2015), PARP-1 activation leads to the formation of compartments in which PAR polymer and DNA are embedded (Figure 1A). When PARP-1 was not activated, no compartment was formed, which indicates that the PAR:FUS interaction is critical to trigger the compartmentalization (Figure 1A).

Nuclear mRNA being the main target of FUS, we then suspected that the presence of mRNA may abrogate the formation of compartments containing PAR, FUS, and DNA. FUS displays a moderate preference for short and redundant RNA sequences in cells but binds to long mRNA in a nonspecific manner *in vitro* (Wang et al., 2015). Therefore, to mimic the binding of FUS to mRNA, we used synthetic mRNA (~3,000 nt) that, in addition, are easily distinguished from DNA and PAR by AFM (Figure S1A). Preforming mRNA:FUS complexes do not affect the capacity of FUS to form DNA-rich compartments after PARP-1 activation. In addition, height measurements of mRNA molecules lying outside large molecular assemblies indicate that the binding of FUS to PAR may be strong enough to displace FUS from mRNA (Figure 1B). In contrast, PAR does not release HuR, an mRNA-binding protein with three RRMs (Mukherjee et al., 2011), from mRNA similarly (Figure 1B). To further probe whether PAR affects the binding of FUS to mRNA, we analyzed the binding of FUS to mRNA using gel mobility shift assay in the presence or absence of free PAR (Figure 1C). As FUS forms large granules in the presence of mRNA, mRNA does not enter the gel. However, the addition of free PAR after the formation of FUS:mRNA complexes impairs mRNA:FUS interactions. PAR and mRNA, therefore, compete for the binding to FUS.

FUS Binds to PAR Synthesized at DNA Damaged Sites after PARP-1 Activation Leading to the Formation of Damaged DNA-Rich Compartments

The recruitment of FUS to DNA damage sites upon PARP-1 activation may provide a means to organize and concentrate DNA repair factors where and when they are most needed. In this model, FUS has to bind PAR when autoPARylated PARP-1 is still anchored to damaged DNA and then forms a compartment

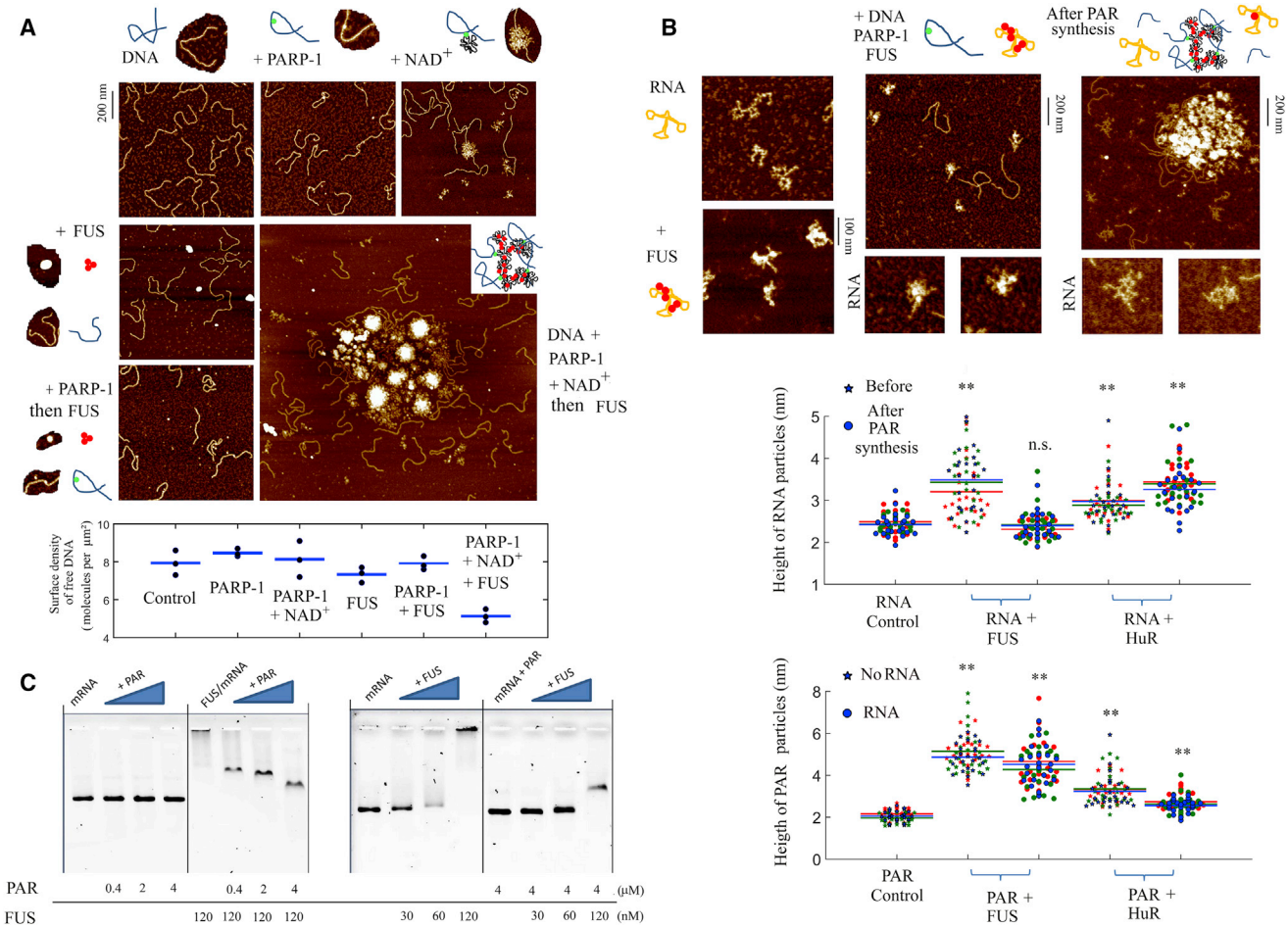

Figure 1. FUS Forms DNA-Rich Compartments upon PARP-1 Activation

(A) Upper panels: AFM images of 1,200-bp nicked DNA (1.25 nM) after incubation with PARP-1 (3 nM) for 5 min in the presence or absence of NAD^+ (0.3 mM) to trigger the synthesis of PAR. The nicked DNA was also pre-incubated with PARP-1 and NAD^+ for 5 min, followed by the addition of FUS (40 nM) and incubation for 1 min. Lower panel: surface density of free DNA molecules measured by AFM as indicated. Horizontal bars indicate mean; scanned area: 20 μm^2 per sample, 3 samples per condition. Note the formation of large DNA-rich assemblies and, consistently, the decrease in free DNA density in the presence of FUS but only after PAR synthesis by PARP-1.

(B) Upper panels: FUS and mRNA (40 nM and 2 nM, respectively) were first mixed to form ribonucleoprotein complexes, as indicated. Then, we analyzed the putative binding of FUS to mRNA in the presence of 1200-bp nicked DNA with or without PARP-1 activation. Note that PAR synthesis leads to the apparent dissociation of FUS:mRNA complexes. Lower panels: heights of mRNA or PAR particles were measured under the indicated conditions in the presence of either HuR or FUS (40 nM each). PAR disrupts RNA:FUS but not RNA:HuR complexes. **$p < 0.05$, paired t test; $n = 25$ per sample. Different colors represent independent experiments.

(C) Agarose gels showing the electrophoretic mobility of mRNA in the presence of FUS and/or free PAR. mRNA (0.8 nM) was pre-incubated with either FUS or free PAR for 10 min at indicated concentrations. The presence of mRNA in the well is due to the formation of mRNA:FUS granules. PAR clearly affects the electrophoretic mobility of mRNA:FUS complexes, whether preformed or not.

enriched in DNA damage sites. To test this model, we first probed whether PAR alone is sufficient to form FUS-PAR compartments in order to discard the role of the binding of FUS to damaged DNA or PARP-1 in this process. In the presence of free PAR, FUS retains its ability to form large FUS-PAR compartments (Figure 2A). We then examined whether free FUS-PAR compartments have an affinity for damaged plasmid DNA (pBR) in the presence of PARP-1 but without NAD^+ to prevent PAR synthesis. Under such conditions, the damaged DNA molecules were mostly found away from FUS-PAR compartments. In contrast, the activation of PARP-1 at DNA damage sites leads to the enrichment of damaged DNA inside FUS-PAR compartments (Figure 2B). FUS most probably binds to PAR newly synthesized by PARP-1 and then subsequently forms large compartments in which damaged DNA is entrapped. To confirm this point, activated PARP-1 was incubated with damaged DNA for a longer time to induce the progressive release of auto-PARylated PARP-1 from damaged DNA (Sukhanova et al., 2016). Accordingly, the enrichment of damaged DNA found inside FUS-PAR compartments was reduced when the addition of FUS was delayed (Figure S1B). Moreover, when PARG was used to hydrolyze PAR prior to mixing FUS with

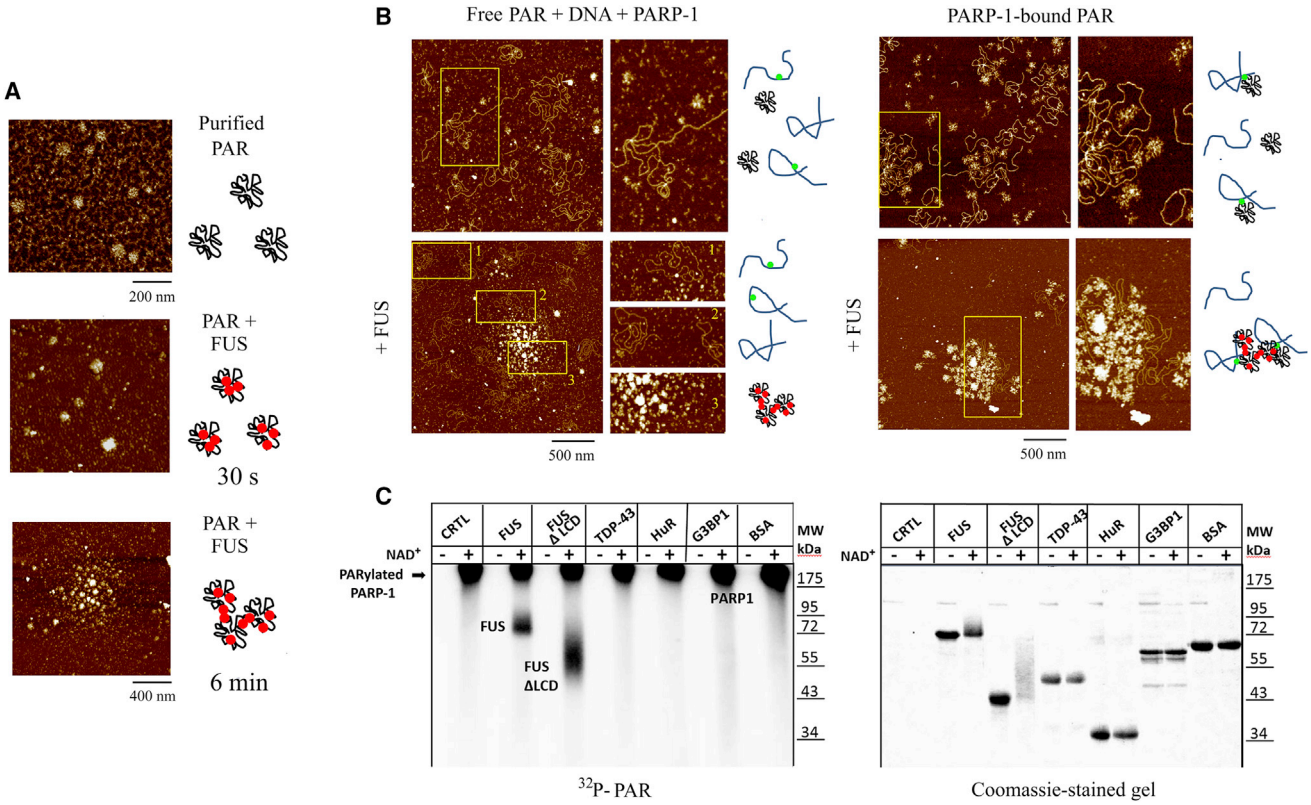

Figure 2. After PARP-1 Activation, FUS Is PARylated at DNA Damage Sites and Forms Compartments

(A) Representative AFM images of PAR:FUS complexes at different incubation times. PAR: 1 μM; FUS: 40 nM. We observed the progressive formation of large FUS:PAR assemblies.

(B) The formation of DNA-rich compartments by FUS was probed in the presence of either free PAR or PAR attached to PARP-1 after incubation with damaged pBR (1.25 nM) and NAD^+ (0.3 mM). Multiple DNA damage sites were generated in plasmid DNA to induce PARP-1 activation and increase the level of PAR synthesis (see the Methods Details section in STAR Methods). The formation of damaged DNA-rich compartments requires both the activation of PARP-1 and the presence of FUS.

(C) Analysis of the PARylation of RNA-binding proteins (0.1 μg/μL each) by PARP-1 (50 nM) in the presence of DNase-activated DNA and [^{32}P]-NAD^+ (0.4 μCi). The reaction mixtures were analyzed by SDS-PAGE with subsequent phosphorimaging (left panel) and Coomassie blue staining (right panel). Note the PARylation of FUS in contrast to other tested proteins (see also Figure S2).

damaged DNA (Figure S1C), the assembly of damaged DNA compartments no longer took place, further suggesting the critical role of the synthesis of long PAR chains in the assembly of these compartments.

However, direct evidence that FUS binds to PAR synthesized by PARP-1 at DNA damage sites was still lacking. We then supposed that the recruitment of FUS to PAR when PARP-1 is activated at DNA damage sites should result in the PARylation of FUS by PARP-1, due to their close proximity. In contrast to other RNA-binding proteins, TDP-43, HuR, and G3BP1, FUS was, indeed, PARylated by PARP-1 in the presence of damaged DNA and NAD^+ (Figures 2C and S2). In addition, the PARylation of FUS by PARP-1 also takes place after truncation of the LCD of FUS. As the RGG and/or RRM domains of FUS bind to PAR, these domains probably undergo PARylation by PARP-1.

Finally, to explore the notion that FUS can concentrate DNA damage sites into FUS-PAR compartments, a solution containing damaged (relaxed or linear) and supercoiled (intact) pBR plasmids was prepared prior to PAR synthesis catalyzed by PARP-1. Upon PARP-1 activation, FUS gathered many plasmid DNAs inside large compartments whose DNA composition was analyzed (Figure 3A). Isolated supercoiled and damaged plasmid DNAs can be clearly identified by AFM. By measuring the ratio of supercoiled to relaxed or linear DNA lying outside compartments, we found that damaged DNA is preferentially located in compartments formed by FUS after PAR synthesis by PARP-1 (Figure 3A). To further explore this point, we performed a co-sedimentation assay in the presence of FUS and a mixture of linear plasmid DNAs (damaged and undamaged; Figures 3 and S3). FUS preferentially co-sediments with DNA with multiple damage sites as long as PARP-1 synthesizes PAR from NAD^+ (Figure 3B). Consistently, while experiments performed under similar conditions do not give exactly similar results, the variability is not significant compared to the large increase in damaged DNA found in the pellet in the presence of FUS after PARP-1 activation (Figure 3B). In addition, co-sedimentation of damaged DNA with FUS does not depend on DNA sequences, as similar results were obtained after permuting plasmid DNAs

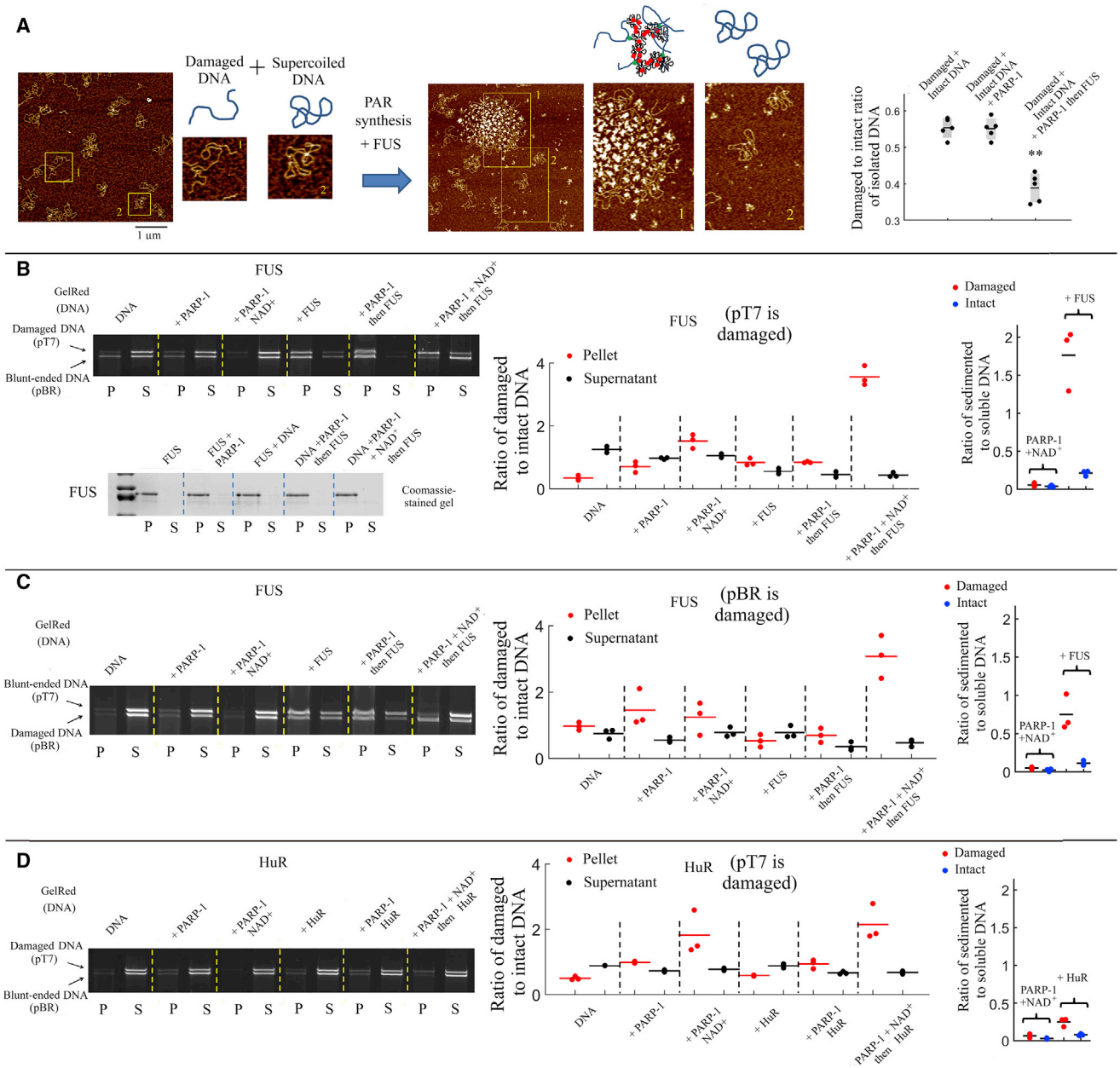

Figure 3. FUS Forms Compartments in Which Damaged DNA Is Enriched

(A) Left panel: an equimolar ratio of supercoiled and damaged pBR (0.625 nM each) was incubated with PARP-1 in the presence of NAD^+ for 5 min to synthesize PAR. Then, the formation of DNA-rich compartments was analyzed by AFM after the addition of FUS and incubation for 1 min. Right panel: the ratio of damaged to supercoiled plasmid DNA detected outside compartments was then measured (**$p < 0.05$, paired t test; n = 5; mean of 5 independent samples, n = 100 molecules per sample). Note that the surface density of damaged pBR located outside compartments decreases relatively to supercoiled pBR.

(B) Right panel: co-sedimentation of FUS with linear plasmid DNAs (damaged pT7 and undamaged pBR) before and after PARP-1 activation in the presence of NAD^+. An equimolar ratio (1 nM each) of pBR (4.36 kb) and pT7 (5.35 kb) were incubated with 10 nM PARP-1 and NAD^+ in the presence of 1 μM FUS. P, pellet; S, supernatant. Left panels: quantitative measurements of the ratio of damaged to intact DNA in pellets and in supernatants obtained from 3 independent experiments shown in Figure S3A. The ratio of sedimented to soluble DNA (damaged and intact) after PARP1 activation in the presence or absence of FUS is also displayed. Damaged DNA preferentially co-sediments with FUS after PARP-1 activation.

(C) Co-sedimentation performed under similar conditions as described as (B) but using an equimolar ratio of linear damaged pBR and linear pT7 and FUS (0.7 μM). Independent experiments are shown in Figure S3C.

(D) Co-sedimentation performed under similar conditions as described as (B) but using HuR (1 μM) instead of FUS. Independent experiments are shown in Figure S3B.

in which multiple damages were generated (Figure 3C). In an additional control experiment, damaged DNA is less efficiently brought into the pellet when HuR, compared with FUS, was added after PARP-1 activation (Figures 3B and 3D; see the ratio of sedimented to soluble DNA for damaged DNA). The ratio of damaged to intact DNA in the pellet also increases significantly in the presence of FUS, which is not observed in the presence of HuR (compare PARP-1 + NAD^+ with and without HuR or FUS; Figures 3B and 3D).

Both the N-Terminal LCD and C-Terminal RGG Domains of FUS Contribute to the Formation of Damaged DNA Compartments

To understand the molecular mechanism leading to the formation of damaged DNA-rich compartments by FUS, we compared the capacity of FUS and that of two other RNA-binding proteins, HuR and G3BP-1, to bind to PAR and form compartments after PARP-1 activation on 1,200-bp nicked DNA. HuR and G3BP-1 also bind to PAR but failed to trigger the formation of large DNA-rich compartments (Figures 4B and 4D). Consistent with this result, FUS sediments more damaged plasmid DNA (pBR) than HuR after the activation of PARP-1 at DNA damage sites (Figures 3B and 3D). A self-attracting LCD, which is present in FUS but not in G3BP1 and HuR, may promote compartmentalization of damaged DNA. To test this hypothesis, a truncated version of FUS (FUSΔLCD), in which most of the N-terminal LCD of FUS was missing, was produced to impair the capacity of FUS to form large damaged DNA compartments (Figure 4A). After this deletion, the formation of large compartments is impaired (Figures 4B and 4D).

Given the critical role of the N-terminal LCD, we prepared recombinant FUS mutants containing six (FUS-6E) or 12 (FUS-12E) mutations of serine or threonine to glutamic acid, mimicking LCD phosphorylation by DNA-PK, as previously described (Monahan et al., 2017) (Figure 4A). The six mutations in the FUS LCD generated small but still noticeable damaged DNA-rich compartments, while 12 mutations totally abrogated the compartmentalization (Figures 4C and 4E). Co-sedimentation assays confirmed the progressive decrease in compartmentalization efficiency by increasing the number of mutations in the LCD (Figures 4E and S4).

An electrostatic interaction between the C-terminal RGG repeats of FUS and PAR has been previously reported *in vitro* (Altmeyer et al., 2015). FUS possesses two RGG domains in its C terminus but also another one between the LCD and the RRM (aa 165–267) (Figure 4A). We then probed whether the C-terminal RGG domains play a key role in damaged DNA compartmentalization by binding FUS to PAR. Two truncated FUS mutants missing either one (FUSΔRGG1) or two (FUSΔRGG1-2) C-terminal RGG repeats were prepared (Figure 4A). Observations through AFM indicate that truncations of the two C-terminal RGG repeats inhibit the formation of compartments (Figure 4C), which was again confirmed by co-sedimentation assay (Figure 4E). The C-terminal RGG repeats are, thus, necessary to fully capture the compartmentalization of damaged DNA, most probably due to the high affinity of RGG repeats for PAR that provides a strong basis for forming large molecular assemblies. However, we noticed that the binding of FUSΔRGG1 to PAR is still significant (Figure 4D). Therefore, although FUSΔRGG1 has an intact LCD and a preserved binding to PAR, its capacity to form compartments is impaired (Figures 4C and 4E). A possible explanation is that multivalent interactions between C-terminal RGG repeats and N-terminal LCD domains play a key role in the compartmentalization process mediated by FUS, as recently reported (Wang et al., 2018b). To further test this hypothesis, we performed a similar analysis with mRNA granules formed in the presence of FUS (Figure 4F). As a control, full-length FUS has the capacity to form large mRNA-rich assemblies. Both truncations of the C-terminal RGG repeats and mutations mimicking the phosphorylated form of the FUS LCD impaired the capacity of FUS to form large mRNA-rich molecular assemblies. Interestingly, while the affinity of FUSΔRGG1-2 for mRNA appears as strongly reduced in gel shift assays, FUSΔRGG1 still binds to PAR significantly (Figure 4D). Again, if LCD was the only domain responsible for the self-attraction between mRNAs bound by proteins, we would have detected large mRNA granules in the presence of FUSΔRGG1. Altogether, these results point toward C-terminal RGG repeats and LCDs driving together large molecular assemblies, but, in addition, the RGG domains participate in the competitive binding of FUS to PAR and mRNA through electrostatic interactions.

PARG Dissociates Damaged DNA-Rich Compartments *In Vitro* and Its Activity Correlates with the Shuttling of FUS from the Nucleus to the Cytoplasm in H_2O_2-Treated HeLa Cells

Single-cell analysis after laser beam damage has revealed the reversible recruitment of FUS to DNA damage sites and a delayed dissociation of FUS-rich compartments at damage DNA sites after the silencing of PARG expression (Altmeyer et al., 2015; Patel et al., 2015). More recently, a PARG-dependent nucleocytoplasmic shuttling of FUS has been reported in neurons (Naumann et al., 2018). PARG may thus be directly responsible for the release of FUS from damaged DNA regions and the subsequent FUS translocation to the cytoplasm. However, phosphorylation of FUS by DNA-PK and, possibly, other kinases may also promote FUS translocation in response to DNA damages (Deng et al., 2014; Naumann et al., 2018). In addition, arginine methylation modulates the binding of transportin to FUS (Dormann et al., 2010), its nuclear import (Dormann et al., 2012), and inhibits the liquid-liquid phase separation of FUS (Hofweber et al., 2018; Qamar et al., 2018).

We then asked whether the translocation of FUS in cells is consecutive to the dissociation of FUS-rich compartments in damaged DNA regions in cells. To answer this question, we decided to explore the fate of FUS in HeLa cells following its transient recruitment to DNA damage sites and its putative release upon PAR hydrolysis by PARG at different times after cell exposure to H_2O_2. We chose H_2O_2 treatment that results in massive PAR synthesis (Figure 5A). The subcellular locations of FUS or other nuclear RNA-binding proteins—HuR, TIA-1, SF1 and TDP-43—were measured (Figure 5A). Solely TDP-43 and FUS shuttle from the nucleus to the cytoplasm after a 90-min incubation (Figure 5A). To test the role of PAR synthesis in this process, cells were pretreated with a specific inhibitor of PARP-1 and PARP-2, olaparib. FUS, but not TDP-43, translocation was

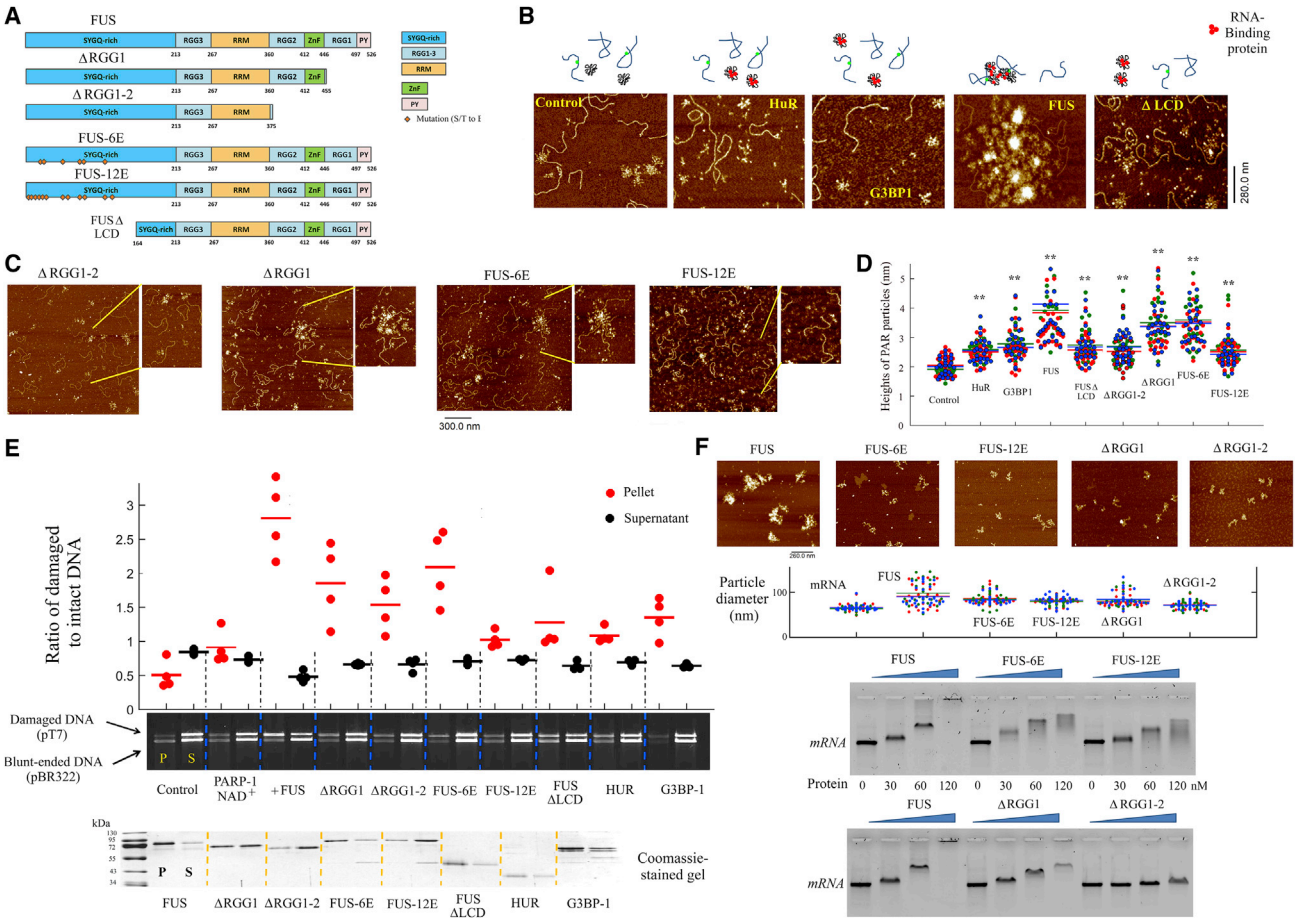

Figure 4. Either Phosphorylation in the N-Terminal LCD or Truncation of the C-Terminal RGG Domains Impairs the Formation of DNA Compartments

(A) FUS constructs and mutations used in this study.

(B) 1,200-bp nicked DNA (1 nM) was pre-incubated with PARP-1 and NAD^+ before the addition of indicated mRNA-binding proteins (40 nM). Full-length FUS is the only protein that generates the formation of large DNA-rich molecular assemblies.

(C) Same as in (B), with indicated FUS mutants.

(D) Measurement of PAR particle heights in the presence of indicated proteins by atomic force microscopy (horizontal bars indicate mean; n = 27 per samples, 3 samples per condition represented with a different color). $^{**}p < 0.05$, paired t test.

(E) Co-sedimentation of mRNA-binding proteins with linear plasmid DNAs (damaged pT7 and undamaged pBR) after PARP-1 activation in the presence of NAD^+. Damaged pT7 and undamaged pBR (1 nM each) were incubated with PARP-1 (10 nM) and NAD^+ (0.3 mM) in the presence of indicated protein (1 μM). P, pellet; S, supernatant. The ratios of damaged to intact DNA measured in pellets and supernatants were obtained from the independent experiments shown in Figure S4.

(F) Upper panels: AFM images of mRNA (2 nM) incubated with indicated FUS mutants (40 nM) for 10 min to probe the formation of mRNA-rich granules by AFM. The scatterplots represent the diameter of mRNA particles for the indicated conditions (horizontal bars indicate mean; n = 27 per sample, 3 samples per condition represented with a different color). Full-length FUS formed large molecular assemblies in the presence of mRNA, while both truncations of the RGG domain and phosphorylation events in the FUS LCD affect the formation of mRNA granules *in vitro*. Lower panels: agarose gels showing the electrophoretic mobility of mRNA in the presence of FUS mutants. mRNA (0.8 nM) was pre-incubated with either FUS or mutants at the indicated concentrations for 10 min. The presence of mRNA in the well is due to the formation of mRNA:FUS granules.

dependent on PAR synthesis (Figures 5B, 5C, and S5B). The translocation of FUS after H_2O_2 exposure was confirmed with two different antibodies and in GFP-FUS-expressing cells (Figure S5A). Furthermore, decreased expression of PARP-1 suppresses the translocation of FUS in H_2O_2-treated cells (Figure 5B). Interestingly, in contrast to TDP-43, the level of cytoplasmic FUS rather decreases at the early stage after stress (15 min, PARylation spike) and increases solely after longer incubation times (30 and 90 min), reflecting the initial recruitment of FUS to DNA damage sites. We then examined why we did not observe the nucleocytoplasmic shuttling of HuR after H_2O_2 treatment while a PARP-dependent translocation of HuR was recently reported after a long lipopolysaccharide exposure (Ke et al., 2017). To address this point, we used actinomycin D (ActD), a transcription inhibitor that is particularly efficient in inducing the rapid translocation of HuR to the cytoplasm (Bounedjah et al., 2014). H_2O_2 treatment prevents HuR translocation triggered by ActD (Figure 5D). Inhibiting of PARP activity restores

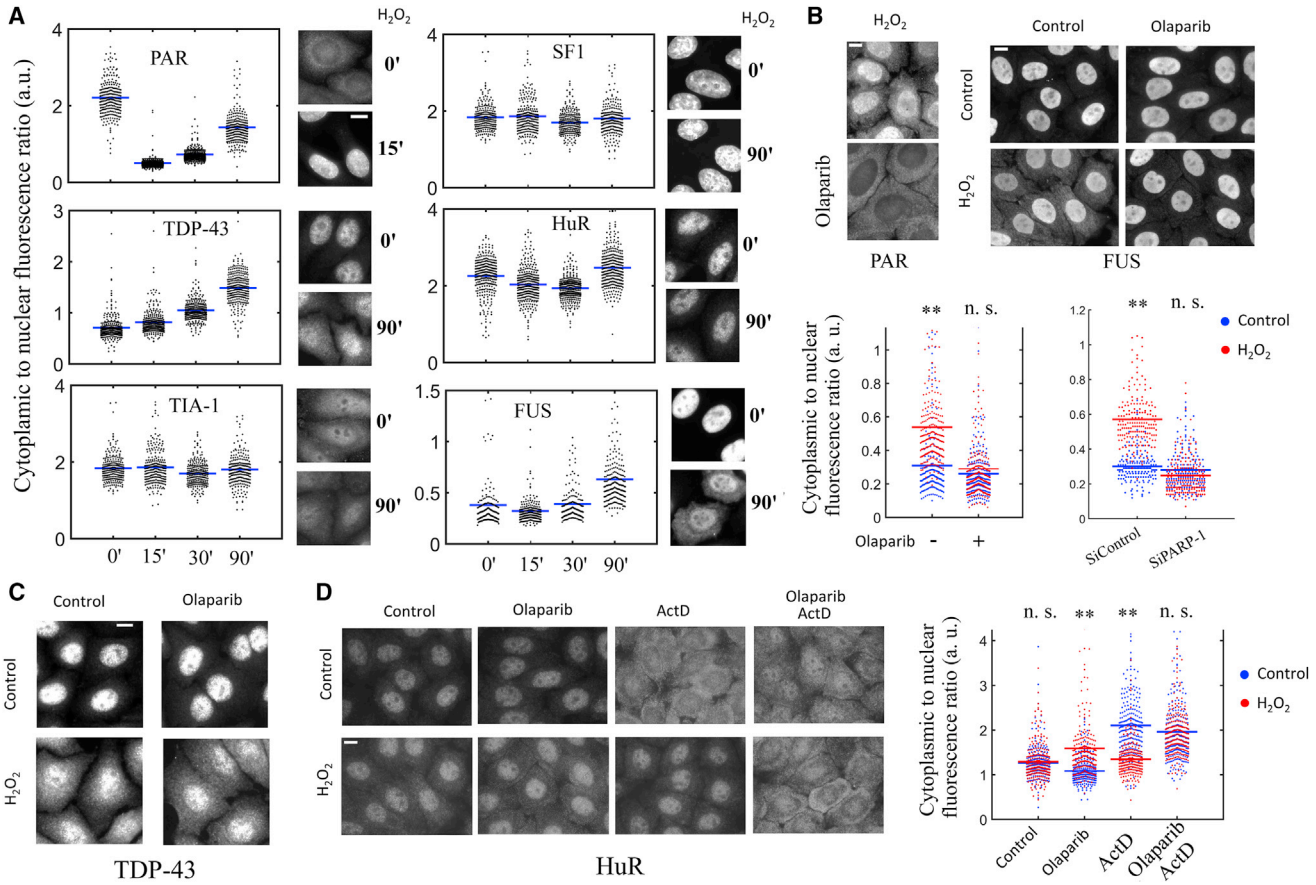

Figure 5. FUS, but Not TDP-43, HuR, SF1, or TIA-1, Shuttles from the Nucleus to the Cytoplasm after PARP-1 Activation in H_2O_2-Treated Cells

(A) The relative distribution of PAR and five other RNA-binding proteins—SF1, TDP-43, TIA-1, FUS, and HuR—between the cytoplasm and nucleus of HeLa cells was measured at different times after H_2O_2 treatment (300 μM). The integrated fluorescence intensities were measured at the single-cell level by using cell profiler software and secondary antibody fluorescence. Statistical analysis of protein translocation was performed under the indicated conditions. Horizontal bars indicate mean; n > 244. Note that FUS translocation takes place after 15 min, which is not observed for TDP-43.

(B) Upper left panel: anti-PAR fluorescence after H_2O_2 treatment (300 μM) for 10 min in the presence or absence of olabarib (10 μM). Upper right panels: subcellular FUS distribution after the indicated treatments. Lower panels: statistical analysis of FUS translocation under indicated conditions. H_2O_2 treatment: 300 μM, 90 min. Horizontal bars indicate mean. **$p < 0.05$, paired t test; n.s., non-significant; n > 278. Olaparib treatment or silencing PARP-1 inhibits the shuttling of FUS from the nucleus to the cytoplasm.

(C) Subcellular distribution of TDP-43 in HeLa cells under the same conditions as in (B). Olaparib does not impair the nucleocytoplasmic shuttling of TDP-43.

(D) Left panels: subcellular distribution of HuR in HeLa cells under the indicated conditions. Right panel: analysis of the nucleocytoplasmic shuttling of HuR. **$p < 0.05$, paired t test; n = 240. Actinomycin D, ActD: 5 μg/mL. Scale bar, 10 μm. H_2O_2 treatment prevents the translocation of HuR in response to ActD in HeLa cells in a PAR-dependent manner. n.s., not significant.

HuR translocation after H_2O_2 treatment. PARP-1 activation thus disrupts the signalization pathways (Doller et al., 2008) related to HuR translocation from the nucleus to the cytoplasm. In summary, FUS relocates to the cytoplasm in response to H_2O_2 treatment after 15 min, when the nuclear PAR level starts to decrease, but not before. In addition, we demonstrate the specific behavior of FUS since, among the five RNA-binding proteins tested here, only the nucleocytoplasmic shuttling of FUS is promoted by the synthesis of PAR in H_2O_2-treated cells.

The correlation between decreasing PAR level and FUS translocation (Figure 5A) suggests that the hydrolysis of PAR by PARG may release FUS from DNA damage sites, thus promoting its translocation to the cytoplasm. To test this hypothesis, we analyzed the subcellular distribution of FUS at the single-cell level after having decreased PARG expression (Figure S6) at different times after cell exposure to H_2O_2. We found that decreased PARG level has dual consequences on FUS translocation (Figure 6A). On the one hand, decreased PARG level slightly promotes FUS translocation from the nucleus to the cytoplasm (the mean cytoplasmic to nuclear fluorescence ratio of anti-FUS antibody increases from 0.66 a.u. ± 0.28 a.u. to 0.77 a.u. ± 0.29 a.u., for control Small interfering RNA (siRNA) and SiPARG, respectively, after H_2O_2 exposure for 90 min). Higher levels of PAR in PARG-silenced cells than in control cells enhance the recruitment of FUS to DNA damage sites. In addition, the remaining PARG activity may be sufficient to cleave long PAR into short chains, thus enabling the release of FUS from DNA damage sites. For these two reasons, the subsequent

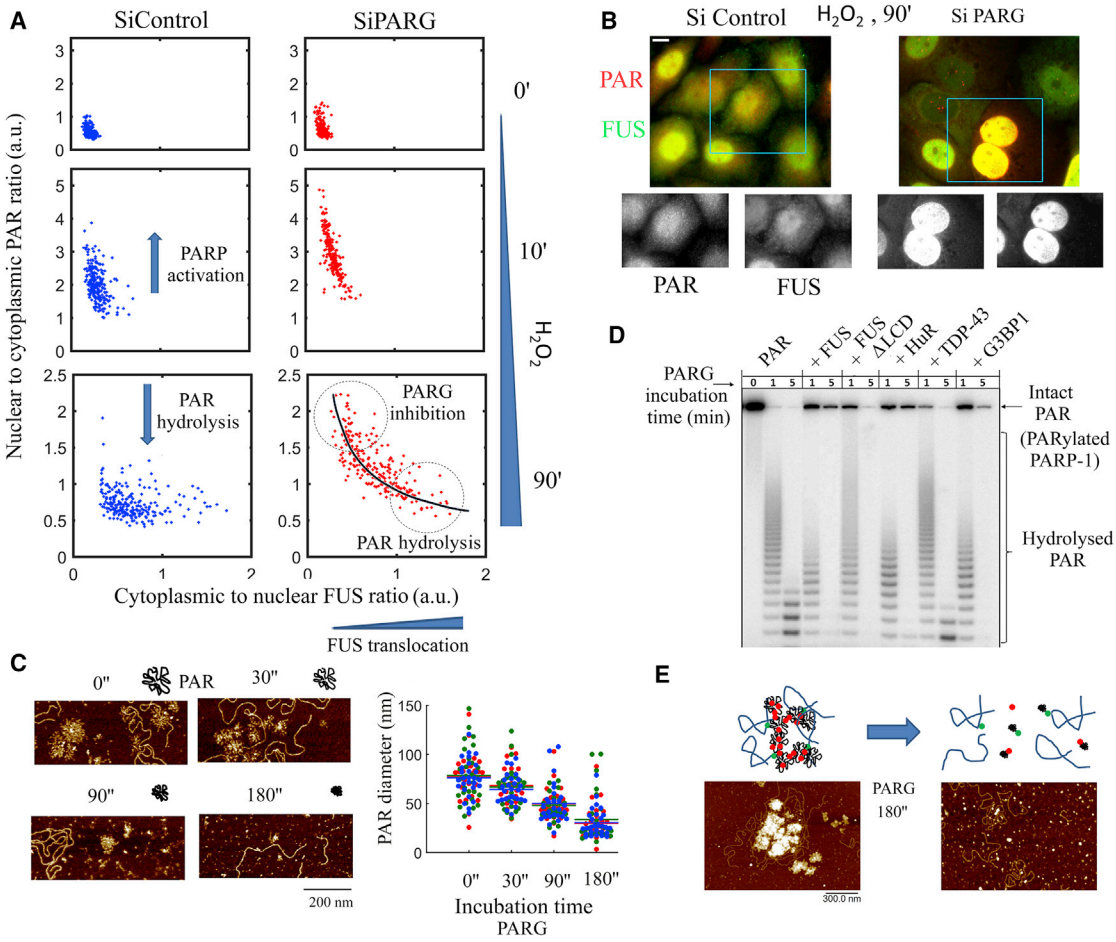

Figure 6. PARG Dissociates DNA-Rich Compartments and Favors FUS Translocation

(A) Nuclear to cytoplasmic PAR ratio (nuclear PAR level) and cytoplasmic to nuclear ratio of FUS (FUS translocation) after different exposure times (H_2O_2, 300 μM) in HeLa cells treated with SiPARG or control siRNA. The polynomial curve shows the correlation between PAR digestion by PARG and FUS translocation.

(B) HeLa cells were treated with SiPARG or control siRNA and then exposed to 300 μM H_2O_2 for the indicated time. The presence of a bright anti-PAR signal in some nucleus of cells treated with SiPARG is most probably due to a lower PARG activity. Staining: anti-PAR (red) and anti-FUS (green) antibodies. Scale bar, 10 μm.

(C) AFM images of PAR degradation by PARG. PAR synthesized by PARP-1 in the presence of damaged pBR was digested by PARG (4 nM) for the indicated times. The diameter of PAR particles was measured under the indicated conditions. Statistical analysis: horizontal bars indicate mean; n = 27 for each sample, 3 samples per condition shown with a different color.

(D) PAGE analysis of PAR degradation by PARG in the presence of RNA-binding proteins. PARP-1 (30 nM) was incubated with damaged pBR (3 nM) in the presence of [^{32}P]-NAD followed by incubation with PARG (4 nM) for 1–5 min in the absence or presence of indicated mRNA-binding proteins (2.4 μM) for the indicated time. The products of hydrolysis of PAR were analyzed by denaturing 10% PAGE with subsequent phosphorimaging.

(E) Representative AFM images of damaged DNA-rich compartments prior to or after the hydrolysis of PAR by PARG. Compartments were preformed after PARP-1 activation and FUS addition. PARG dissociates preformed DNA-rich compartments.

release of FUS from damaged DNA may be, on average, more efficient when PARG is partially silenced. On the other hand, analyzing the correlation between FUS translocation and the PAR level at the single-cell level revealed that elevated PAR levels in nucleus inhibit the FUS translocation after 90 min of H_2O_2 exposure (Figures 6A and 6B). We hypothesized that cells displaying elevated levels of PAR in nucleus at this time are actually the ones for which PARG activity is not sufficient to release FUS from DNA damage sites. This observation confirms the notion that PARG activity is required for the translocation of FUS from the nucleus to the cytoplasm.

To challenge this hypothesis, we considered whether damaged DNA-rich compartments formed by FUS *in vitro* can be readily dissociated by recombinant PARG. After demonstrating that recombinant PARG hydrolyzes PAR *in vitro* (Figure 6C), we analyzed whether FUS protects PAR from degradation by PARG. FUS, to a similar extent than other mRNA-binding proteins, indeed, partly protects PAR from hydrolysis. However, most of PAR is clearly hydrolyzed, despite the presence of FUS (Figure 6D). We then probed the consequences of PARG activity on preformed DNA-rich compartments formed after the activation of PARP-1 and in the presence of FUS (Figure 6E). *In vitro*,

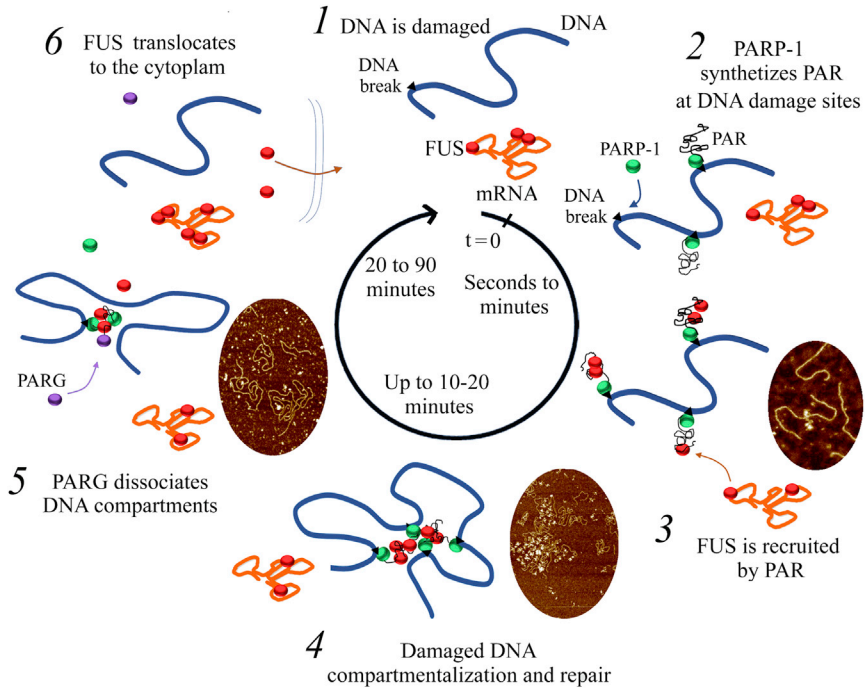

Figure 7. Schematic View of the Different Steps of Damaged DNA Compartmentalization by FUS

PARG induces the rapid dissociation of damaged DNA compartments, as evidenced by the appearance of isolated DNA molecules. Thus, PARG activity is sufficient to dissociate damaged DNA-rich compartments *in vitro*, which possibly contributes to the shuttling of FUS from the nucleus to the cytoplasm.

As AFM results reveal that both FUS phosphorylation in the N-terminal LCD and truncations of the C-terminal RGG repeats antagonize the formation of damaged DNA-rich compartments (Figures 4C and 4E), it is therefore tempting to speculate that FUS phosphorylation and/or arginine methylation may as well control the reversibility of these compartments.

DISCUSSION

The putative functions attributed to PAR synthesis in the nucleus are numerous, among which are unlocking the histone-driven compaction of chromatin, signaling functions, and recruiting DNA repair factors. Here, we explored the role of PARP-1 activated by DNA damages in the redistribution of RNA-binding proteins (Altmeyer et al., 2015; Izhar et al., 2015), which could have functional consequences in DNA repair (Wang et al., 2013) but also in the ensuing translational response to stress (Leung et al., 2011). Based on its high PARylation level after genotoxic stress (Jungmichel et al., 2013) and its early PAR-dependent recruitment to DNA damage sites (Rulten et al., 2014), we focused this study on FUS. Through a single-molecule approach *in vitro*, we reconstituted the molecular system including FUS, mRNA to mimic nuclear mRNA targets of FUS, damaged DNA, PARP-1 (to recognize DNA damages sites), NAD^+ (to trigger the synthesis of PAR by PARP-1), and PARG (to hydrolyze PAR). We demonstrate the strong affinity of FUS for PAR, which can then successfully compete with mRNA for the binding to FUS (Figures 1B and 1C), the recruitment of FUS to PAR synthesized by PARP-1 at DNA damage sites, and the formation of large compartments in which damaged DNA is concentrated (Figures 2B, 3A, and 3B). FUS, thus, generates dynamic compartments in which damaged DNA accumulates, which should facilitate the recognition of damaged DNA by DNA repair factors due to the relative decrease in undamaged DNA concentration within the compartments. This function cannot be fulfilled by PAR alone, due to its inability to self-attract, in contrast to the multivalent interactions taking place in the LCD and RGG repeats of FUS. Interestingly, phosphorylation of the FUS LCD impairs the formation of liquid-like compartments (Monahan et al., 2017; Murray et al., 2017) and, accordingly, inhibits the formation of damaged DNA-rich compartments, suggesting an important role for kinases such as DNA-PK in regulating their formation. Arginine methylation of the RGG domains may be also finely regulating the assembly of DNA damaged compartments by decreasing the affinity of FUS for PAR or by tuning multivalent interactions between the C-terminal RGG domain and the N-terminal LCD (Bogaert et al., 2018; Wang et al., 2018b).

Having evidenced the capacity of FUS to segregate damaged DNA from intact DNA in liquid-like compartments, we wondered whether it could provide an advantage in the process of DNA repair in cells. After exposure to H_2O_2, mammalian cells rejoin DNA strand breaks rapidly ($t_{1/2}$, ~15 min for HeLa cells) (Lorenzo et al., 2009). During this time interval (<30 min), there might be a kinetic advantage to gather damaged DNA sites (Figure 7). Concentrating DNA repair factors where they are most needed should increase the rate of DNA repair. Chromatin mobility is, indeed, reduced (Liu et al., 2015) or corralled in small volumes (Jakob et al., 2009) just after PARP-1 activation (<30 min). These observations are in agreement with the participation of FUS and possibly other RNA-binding proteins in DNA repair, notably in neurons (Wang et al., 2013). Most of the experimental data obtained so far were focused on late chromatin mobility after double-strand DNA break formation, which induces homology search during homologous recombination. However, a clustering of DNA DSBs repaired by non-homologous end joining in cells has been proposed to generate repair domains that could be essential for rapid DNA repair (Schrank et al., 2018). Similarly, PAR, together with FUS, may shape chromatin organization to form transient compartments in which damaged DNA repair that does not require homologous recombination is processed effectively and rapidly.

We also demonstrate at the single-molecule level that, after an initial PAR-dependent recruitment of FUS on DNA damage sites, FUS—but not other mRNA-binding proteins, TDP-43, G3BP-1, and HuR—is highly PARylated by PARP-1 *in vitro* (Figure 2C), providing an explanation for the preferential PARylation of FUS detected in cells (Britton et al., 2014; Jungmichel et al., 2013; Zhen et al., 2017). FUS is then progressively released from DNA damage sites in cells, this process being orchestrated by PARG (Altmeyer et al., 2015; Naumann et al., 2018; Patel et al., 2015). Incidentally, PARG activity is sufficient to dissociate damaged DNA-rich compartments *in vitro* (Figure 6E). By exploring the fate of FUS after the dissociation of these compartments in HeLa cells after H_2O_2 exposure, we also show evidence that FUS shuttles from the nucleus to the cytoplasm, generalizing recent results found in neurons (Naumann et al., 2018). In addition, the PARP-dependent nucleocytoplasmic shuttling of FUS is not shared by other RNA-binding proteins such as TDP-43, HuR, SF1, or TIA-1 (Figures 5A–5C). As the phosphorylation of FUS LCDs inhibits the capacity of FUS to form damaged-DNA compartments *in vitro* (Figure 4E), we may speculate that DNA-PK may release FUS from these compartments to facilitate FUS translocation. Nevertheless, we do not know whether DNA-PK phosphorylates FUS in preformed damaged-DNA rich compartments and thus acts upstream of PARG activity (Deng et al., 2014; Monahan et al., 2017).

In light of the results presented here, we may also ask whether pathogenic FUS mutations, notably in the RGG repeats, impair DNA repair in damaged DNA-rich compartments and/or the nucleocytoplasmic shuttling of FUS. These issues deserve to be addressed to increase our understanding of the link between DNA repair and neurodegenerative diseases (Hoch et al., 2017; Naumann et al., 2018; Wang et al., 2018a).

STAR★METHODS

Detailed methods are provided in the online version of this paper and include the following:

- KEY RESOURCES TABLE
- CONTACT FOR REAGENT AND RESOURCE SHARING
- EXPERIMENTAL MODEL AND SUBJECT DETAILS
  - Cell culture conditions
  - Cell cultures, transfections and chemicals/drug treatment
  - RNA interference
- METHODS DETAILS
  - Protein production and purification
  - Expression and purification of FUS, FUSΔLCD, TDP-43, HuR, G3BP1, FUS-6E, FUS-12E, FUSΔRGG1 or FUSΔRGG1-2
  - Preparation of DNA Substrates, mRNA and PAR
  - Preparation of samples for atomic force microscopy
  - AFM imaging and image analysis
  - Radioactive assay of protein PARylation and PAR hydrolysis by PARG *in vitro*
  - Analysis of binding of FUS to RNA by EMSA
  - Co-sedimentation assays to probe the enrichment of damaged DNA in FUS/PAR compartments
  - Immunofluorescence analysis
  - Western blot analysis of PARG expression
- QUANTIFICATION AND STATISTICAL ANALYSIS

SUPPLEMENTAL INFORMATION

Supplemental Information can be found online at https://doi.org/10.1016/j.celrep.2019.04.031.

ACKNOWLEDGMENTS

We are grateful to Dr. V. Schreiber (UMR7242 du CNRS École Supérieure de Biotechnologie de Strasbourg, France) for PARG and PARP-1 expression plasmids; Dr. S.H. Wilson (NEIHS, Durham, NC, USA) for the APE-1 expression plasmid; and to Drs. E. Ilina (ICBFM SB RAS, Krasnoyarsk, Russia), S.N. Khodyreva (ICBFM SB RAS, Krasnoyarsk, Russia), and S.I. Shram (IMG RAS, Moscow, Russia) for providing us with PARG, APE-1, and NMNAT preparations. We gratefully acknowledge the Genopole Evry and INSERM for constant support of the laboratory. We thank Dr. R.C. Maroun for interesting comments and corrections. This study was supported by the Russian State-funded budget project of ICBFM SB RAS (AAAA-A17-117020210022-4 to O.I.L.); the Russian Scientific Foundation (RSF 19-14-00107 to O.I.L.); the Russian Foundation for Basic Research (18-04-00882 to M.V.S.); and the Vernadsky program of the French Embassy in the Russian Federation (PhD grant to A.S.S.).

AUTHOR CONTRIBUTIONS

Conceptualization: A.S.S., L.H., M.V.S., O.I.L., and D.P.; Methodology: A.S.S., L.H., M.V.S., B.D., V.J., and A.B.; Validation: A.S.S., L.H., and M.V.S.; Formal Analysis: A.S.S., M.V.S., L.H., O.I.L., and D.P.; Investigation: A.S.S., L.H., and M.V.S.; Resources: A.S.S., L.H., M.V.S., B.D., V.J., and A.B.; Data Curation: A.S.S., M.V.S., and L.H.; Writing – Review & Editing: O.I.L. and D.P.; Visualization: A.S.S., M.V.S., L.H., O.I.L., and D.P.; Supervision: O.I.L. and D.P.; Project Administration: O.I.L. and D.P.

DECLARATION OF INTERESTS

The authors declare no competing interests.

Received: March 19, 2018
Revised: September 21, 2018
Accepted: April 4, 2019
Published: May 7, 2019

REFERENCES

Aguzzi, A., and Altmeyer, M. (2016). Phase separation: linking cellular compartmentalization to disease. Trends Cell Biol. *26*, 547–558.

Altmeyer, M., Neelsen, K.J., Teloni, F., Pozdnyakova, I., Pellegrino, S., Grøfte, M., Rask, M.-B.D., Streicher, W., Jungmichel, S., Nielsen, M.L., and Lukas, J. (2015). Liquid demixing of intrinsically disordered proteins is seeded by poly(ADP-ribose). Nat. Commun. *6*, 8088.

Amé, J.C., Héberlé, É., Camuzeaux, B., Dantzer, F., and Schreiber, V. (2017). Purification of recombinant human PARG and activity assays. Methods Mol. Biol. *1608*, 395–413.

Banani, S.F., Lee, H.O., Hyman, A.A., and Rosen, M.K. (2017). Biomolecular condensates: organizers of cellular biochemistry. Nat. Rev. Mol. Cell Biol. *18*, 285–298.

Bergeron-Sandoval, L.P., Safaee, N., and Michnick, S.W. (2016). Mechanisms and consequences of macromolecular phase separation. Cell *165*, 1067–1079.

Bock, F.J., Todorova, T.T., and Chang, P. (2015). RNA regulation by poly(ADP-ribose) polymerases. Mol. Cell *58*, 959–969.

Bogaert, E., Boeynaems, S., Kato, M., Guo, L., Caulfield, T.R., Steyaert, J., Scheveneels, W., Wilmans, N., Haeck, W., and Hersmus, N. (2018). Molecular

dissection of FUS points at synergistic effect of low-complexity domains in toxicity. Cell Rep. *24*, 529–537.e24.

Bounedjah, O., Desforges, B., Wu, T.D., Pioche-Durieu, C., Marco, S., Hamon, L., Curmi, P.A., Guerquin-Kern, J.L., Piétrement, O., and Pastré, D. (2014). Free mRNA in excess upon polysome dissociation is a scaffold for protein multimerization to form stress granules. Nucleic Acids Res. *42*, 8678–8691.

Britton, S., Dernoncourt, E., Delteil, C., Froment, C., Schiltz, O., Salles, B., Frit, P., and Calsou, P. (2014). DNA damage triggers SAF-A and RNA biogenesis factors exclusion from chromatin coupled to R-loops removal. Nucleic Acids Res. *42*, 9047–9062.

Ciccia, A., and Elledge, S.J. (2010). The DNA damage response: making it safe to play with knives. Mol. Cell *40*, 179–204.

Deng, Q., Holler, C.J., Taylor, G., Hudson, K.F., Watkins, W., Gearing, M., Ito, D., Murray, M.E., Dickson, D.W., Seyfried, N.T., and Kukar, T. (2014). FUS is phosphorylated by DNA-PK and accumulates in the cytoplasm after DNA damage. J. Neurosci. *34*, 7802–7813.

Doller, A., Pfeilschifter, J., and Eberhardt, W. (2008). Signalling pathways regulating nucleo-cytoplasmic shuttling of the mRNA-binding protein HuR. Cell. Signal. *20*, 2165–2173.

Dormann, D., Rodde, R., Edbauer, D., Bentmann, E., Fischer, I., Hruscha, A., Than, M.E., Mackenzie, I.R., Capell, A., Schmid, B., et al. (2010). ALS-associated fused in sarcoma (FUS) mutations disrupt Transportin-mediated nuclear import. EMBO J. *29*, 2841–2857.

Dormann, D., Madl, T., Valori, C.F., Bentmann, E., Tahirovic, S., Abou-Ajram, C., Kremmer, E., Ansorge, O., Mackenzie, I.R., Neumann, M., and Haass, C. (2012). Arginine methylation next to the PY-NLS modulates Transportin binding and nuclear import of FUS. EMBO J. *31*, 4258–4275.

Feric, M., Vaidya, N., Harmon, T.S., Mitrea, D.M., Zhu, L., Richardson, T.M., Kriwacki, R.W., Pappu, R.V., and Brangwynne, C.P. (2016). Coexisting liquid phases underlie nucleolar subcompartments. Cell *165*, 1686–1697.

Gagné, J.P., Pic, E., Isabelle, M., Krietsch, J., Ethier, C., Paquet, E., Kelly, I., Boutin, M., Moon, K.M., Foster, L.J., and Poirier, G.G. (2012). Quantitative proteomics profiling of the poly(ADP-ribose)-related response to genotoxic stress. Nucleic Acids Res. *40*, 7788–7805.

Hamon, L., Pastré, D., Dupaigne, P., Le Breton, C., Le Cam, E., and Piétrement, O. (2007). High-resolution AFM imaging of single-stranded DNA-binding (SSB) protein–DNA complexes. Nucleic Acids Res. *35*, e58.

Hennig, S., Kong, G., Mannen, T., Sadowska, A., Kobelke, S., Blythe, A., Knott, G.J., Iyer, K.S., Ho, D., Newcombe, E.A., et al. (2015). Prion-like domains in RNA binding proteins are essential for building subnuclear paraspeckles. J. Cell Biol. *210*, 529–539.

Hoch, N.C., Hanzlikova, H., Rulten, S.L., Tétreault, M., Komulainen, E., Ju, L., Hornyak, P., Zeng, Z., Gittens, W., Rey, S.A., et al.; Care4Rare Canada Consortium (2017). XRCC1 mutation is associated with PARP1 hyperactivation and cerebellar ataxia. Nature *541*, 87–91.

Hofweber, M., Hutten, S., Bourgeois, B., Spreitzer, E., Niedner-Boblenz, A., Schifferer, M., Ruepp, M.-D., Simons, M., Niessing, D., and Madl, T. (2018). Phase separation of FUS is suppressed by its nuclear import receptor and arginine methylation. Cell *173*, 706–719.e13.

Illuzzi, G., Fouquerel, E., Amé, J.C., Noll, A., Rehmet, K., Nasheuer, H.P., Dantzer, F., and Schreiber, V. (2014). PARG is dispensable for recovery from transient replicative stress but required to prevent detrimental accumulation of poly(ADP-ribose) upon prolonged replicative stress. Nucleic Acids Res. *42*, 7776–7792.

Izhar, L., Adamson, B., Ciccia, A., Lewis, J., Pontano-Vaites, L., Leng, Y., Liang, A.C., Westbrook, T.F., Harper, J.W., and Elledge, S.J. (2015). A systematic analysis of factors localized to damaged chromatin reveals PARP-dependent recruitment of transcription factors. Cell Rep. *11*, 1486–1500.

Jakob, B., Splinter, J., Durante, M., and Taucher-Scholz, G. (2009). Live cell microscopy analysis of radiation-induced DNA double-strand break motion. Proc. Natl. Acad. Sci. USA *106*, 3172–3177.

Jungmichel, S., Rosenthal, F., Altmeyer, M., Lukas, J., Hottiger, M.O., and Nielsen, M.L. (2013). Proteome-wide identification of poly(ADP-ribosyl)ation targets in different genotoxic stress responses. Mol. Cell *52*, 272–285.

Kaneb, H.M., Dion, P.A., and Rouleau, G.A. (2012). The FUS about arginine methylation in ALS and FTLD. EMBO J. *31*, 4249–4251.

Ke, Y., Han, Y., Guo, X., Wen, J., Wang, K., Jiang, X., Tian, X., Ba, X., Boldogh, I., and Zeng, X. (2017). PARP1 promotes gene expression at the post-transcriptiona level by modulating the RNA-binding protein HuR. Nat. Commun. *8*, 14632.

Laemmli, U.K. (1970). Cleavage of structural proteins during the assembly of the head of bacteriophage T4. Nature *227*, 680–685.

Leung, A.K. (2014). Poly(ADP-ribose): an organizer of cellular architecture. J. Cell Biol. *205*, 613–619.

Leung, A.K., Vyas, S., Rood, J.E., Bhutkar, A., Sharp, P.A., and Chang, P. (2011). Poly(ADP-ribose) regulates stress responses and microRNA activity in the cytoplasm. Mol. Cell *42*, 489–499.

Li, P., Banjade, S., Cheng, H.C., Kim, S., Chen, B., Guo, L., Llaguno, M., Hollingsworth, J.V., King, D.S., Banani, S.F., et al. (2012). Phase transitions in the assembly of multivalent signalling proteins. Nature *483*, 336–340.

Li, Y.R., King, O.D., Shorter, J., and Gitler, A.D. (2013). Stress granules as crucibles of ALS pathogenesis. J. Cell Biol. *201*, 361–372.

Liu, J., Vidi, P.A., Lelièvre, S.A., and Irudayaraj, J.M. (2015). Nanoscale histone localization in live cells reveals reduced chromatin mobility in response to DNA damage. J. Cell Sci. *128*, 599–604.

Lorenzo, Y., Azqueta, A., Luna, L., Bonilla, F., Domínguez, G., and Collins, A.R. (2009). The carotenoid beta-cryptoxanthin stimulates the repair of DNA oxidation damage in addition to acting as an antioxidant in human cells. Carcinogenesis *30*, 308–314.

Mastrocola, A.S., Kim, S.H., Trinh, A.T., Rodenkirch, L.A., and Tibbetts, R.S. (2013). The RNA-binding protein fused in sarcoma (FUS) functions downstream of poly(ADP-ribose) polymerase (PARP) in response to DNA damage. J. Biol. Chem. *288*, 24731–24741.

Monahan, Z., Ryan, V.H., Janke, A.M., Burke, K.A., Rhoads, S.N., Zerze, G.H., O'Meally, R., Dignon, G.L., Conicella, A.E., Zheng, W., et al. (2017). Phosphorylation of the FUS low-complexity domain disrupts phase separation, aggregation, and toxicity. EMBO J. *36*, 2951–2967.

Mukherjee, N., Corcoran, D.L., Nusbaum, J.D., Reid, D.W., Georgiev, S., Hafner, M., Ascano, M., Jr., Tuschl, T., Ohler, U., and Keene, J.D. (2011). Integrative regulatory mapping indicates that the RNA-binding protein HuR couples pre-mRNA processing and mRNA stability. Mol. Cell *43*, 327–339.

Murray, D.T., Kato, M., Lin, Y., Thurber, K.R., Hung, I., McKnight, S.L., and Tycko, R. (2017). Structure of FUS protein fibrils and its relevance to self-assembly and phase separation of low-complexity domains. Cell *171*, 615–627.e16.

Naumann, M., Pal, A., Goswami, A., Lojewski, X., Japtok, J., Vehlow, A., Naujock, M., Günther, R., Jin, M., Stanslowsky, N., et al. (2018). Impaired DNA damage response signaling by FUS-NLS mutations leads to neurodegeneration and FUS aggregate formation. Nat. Commun. *9*, 335.

Patel, A., Lee, H.O., Jawerth, L., Maharana, S., Jahnel, M., Hein, M.Y., Stoynov, S., Mahamid, J., Saha, S., Franzmann, T.M., et al. (2015). A liquid-to-solid phase transition of the ALS protein FUS accelerated by disease mutation. Cell *162*, 1066–1077.

Qamar, S., Wang, G., Randle, S.J., Ruggeri, F.S., Varela, J.A., Lin, J.Q., Phillips, E.C., Miyashita, A., Williams, D., and Ströhl, F. (2018). FUS phase separation is modulated by a molecular chaperone and methylation of arginine cation-π interactions. Cell *173*, 720–734.e15.

Rhoads, S.N., Monahan, Z.T., Yee, D.S., Leung, A.Y., Newcombe, C.G., O'Meally, R.N., Cole, R.N., and Shewmaker, F.P. (2018). The prion-like domain of FUS is multiphosphorylated following DNA damage without altering nuclear localization. Mol. Biol. Cell *29*, 1786–1797.

Rulten, S.L., Rotheray, A., Green, R.L., Grundy, G.J., Moore, D.A., Gómez-Herreros, F., Hafezparast, M., and Caldecott, K.W. (2014). PARP-1 dependent

recruitment of the amyotrophic lateral sclerosis-associated protein FUS/TLS to sites of oxidative DNA damage. Nucleic Acids Res. *42*, 307–314.

Sama, R.R., Ward, C.L., and Bosco, D.A. (2014). Functions of FUS/TLS from DNA repair to stress response: implications for ALS. ASN Neuro *6*, pii: 1759091414544472.

Schrank, B.R., Aparicio, T., Li, Y., Chang, W., Chait, B.T., Gundersen, G.G., Gottesman, M.E., and Gautier, J. (2018). Nuclear ARP2/3 drives DNA break clustering for homology-directed repair. Nature *559*, 61–66.

Schreiber, V., Dantzer, F., Ame, J.C., and de Murcia, G. (2006). Poly(ADP-ribose): novel functions for an old molecule. Nat. Rev. Mol. Cell Biol. *7*, 517–528.

Singh, G., Pratt, G., Yeo, G.W., and Moore, M.J. (2015). The clothes make the mRNA: past and present trends in mRNP fashion. Annu. Rev. Biochem. *84*, 325–354.

Strzyz, P. (2016). Organelle dynamics: controlling phase separation of P granules. Nat. Rev. Mol. Cell Biol. *18*, 4.

Sukhanova, M.V., Lavrik, O.I., and Khodyreva, S.N. (2004). [Poly(ADP-ribose) polymerase-1 as a regulator of protein-nucleic acid interactions in the processes responding to genotoxic action]. Mol. Biol. (Mosk.) *38*, 834–847.

Sukhanova, M.V., Abrakhi, S., Joshi, V., Pastre, D., Kutuzov, M.M., Anarbaev, R.O., Curmi, P.A., Hamon, L., and Lavrik, O.I. (2016). Single molecule detection of PARP1 and PARP2 interaction with DNA strand breaks and their poly(ADP-ribosyl)ation using high-resolution AFM imaging. Nucleic Acids Res. *44*, e60.

Teloni, F., and Altmeyer, M. (2016). Readers of poly(ADP-ribose): designed to be fit for purpose. Nucleic Acids Res. *44*, 993–1006.

Wang, W.Y., Pan, L., Su, S.C., Quinn, E.J., Sasaki, M., Jimenez, J.C., Mackenzie, I.R., Huang, E.J., and Tsai, L.H. (2013). Interaction of FUS and HDAC1 regulates DNA damage response and repair in neurons. Nat. Neurosci. *16*, 1383–1391.

Wang, X., Schwartz, J.C., and Cech, T.R. (2015). Nucleic acid-binding specificity of human FUS protein. Nucleic Acids Res. *43*, 7535–7543.

Wang, H., Guo, W., Mitra, J., Hegde, P.M., Vandoorne, T., Eckelmann, B.J., Mitra, S., Tomkinson, A.E., Van Den Bosch, L., and Hegde, M.L. (2018a). Mutant FUS causes DNA ligation defects to inhibit oxidative damage repair in amyotrophic lateral sclerosis. Nat. Commun. *9*, 3683.

Wang, J., Choi, J.-M., Holehouse, A.S., Lee, H.O., Zhang, X., Jahnel, M., Maharana, S., Lemaitre, R., Pozniakovsky, A., Drechsel, D., et al. (2018b). A molecular grammar governing the driving forces for phase separation of prion-like RNA binding proteins. Cell *174*, 688–699.e16.

Zhang, H., Elbaum-Garfinkle, S., Langdon, E.M., Taylor, N., Occhipinti, P., Bridges, A.A., Brangwynne, C.P., and Gladfelter, A.S. (2015). RNA controls PolyQ protein phase transitions. Mol. Cell *60*, 220–230.

Zhen, Y., Zhang, Y., and Yu, Y. (2017). A cell-line-specific atlas of PARP-mediated protein Asp/Glu-ADP-ribosylation in breast cancer. Cell Rep. *21*, 2326–2337.

Zhu, L., and Brangwynne, C.P. (2015). Nuclear bodies: the emerging biophysics of nucleoplasmic phases. Curr. Opin. Cell Biol. *34*, 23–30.

STAR★METHODS

KEY RESOURCES TABLE

REAGENT or RESOURCE	SOURCE	IDENTIFIER
Antibodies		
Mouse monoclonal anti-FUS	Novus Biologicals	Cat#NBP2-52874
Rabbit polyclonal anti-FUS (used only in the Figure S2a)	Novus Biologicals	Cat#NB100-565
Rabbit polyclonal anti-PARP1	Santa Cruz Biotechnology	Cat#sc-7150
Mouse polyclonal anti-HuR	Abcam	Cat#ab54987
Goat polyclonal anti-TIA-1	Santa Cruz Biotechnology	Cat#sc-1751
Mouse monoclonal anti-TDP-43	Santa Cruz Biotechnology	Cat#sc-376532
Rabbit polyclonal anti-PAR	Trevigen	Cat#4336-BPC-100
Mouse monoclonal anti- PARG	Santa Cruz Biotechnology	Cat#sc-398563
Mouse monoclonal anti-Alpha-Tubulin	Abcam	Cat#ab7291
Mouse monoclonal anti-SF1	Invitrogen	Cat#MA5-27159
Goat polyclonal anti-Rabbit IgG (H+L)	Thermo Fisher Scientific	Cat#11012
Goat polyclonal anti-Mouse IgG1	Thermo Fisher Scientific	Cat#21121
Goat anti-Mouse IgG (H+L)	LI-COR	Cat#926-32210
Bacterial and Virus Strains		
Escherichia coli BL21(DE3)	EMD Millipore	Cat#69450
Chemicals, Peptides, and Recombinant Proteins		
Actinomycin D (ActD)	Thermo Fisher Scientific	Cat#11805017
Lipofectamine 2000	Thermo Fisher Scientific	Cat#11668019
SYBR Green II RNA Gel Stain	Thermo Fisher Scientific	Cat#S7564
Nb.BsmI, nicking endonuclease	New England BioLabs	Cat#R0706S
HiScribe T7 High Yield RNA Synthesis Kit	New England BioLabs	Cat#E2040S
PAR Polymer	Trevigen	Cat#4336-100-01
Olaparib (AZD2281, Ku-0059436)	Apexbio Technology	Cat#A4154
Ni-NTA Agarose	QIAGEN	Cat#30210
GelRed	Biotium	Cat #41003
Experimental Models: Cell Lines		
Human: HeLa	ATCC	Cat #CRM-CCL-2
Oligonucleotides		
FlexiTube GeneSolution for PARG	QIAGEN	Cat#GS8505
FlexiTube GeneSolution for PARP1	QIAGEN	Cat#GS14
AllStars Negative Control siRNA	QIAGEN	Cat#1027281
Calf thymus DNA	Sigma	Cat#D4522
Recombinant DNA		
Vector pT7-FLAG-MAT-Tag-2	Sigma	Cat#E5030
Vector pBR322	New England BioLabs	Cat#N3033S
pET-FUS	This paper	N/A
pET-FUS-ΔLCD	This paper	N/A
pET-FUS_1-374	This paper	N/A
pET-FUS_1-454	This paper	N/A
pET-MBP-FUS_FL_6E	Monahan et al., 2017	Addgene #98652
pET-MBP-FUS_FL_12E	Monahan et al., 2017	Addgene #98655
pET-Hur	This paper	N/A
pET-G3BP1	This paper	N/A

(*Continued on next page*)

Continued

REAGENT or RESOURCE	SOURCE	IDENTIFIER
pET-TDP-43	This paper	N/A
pET32a-hPARP-1-His	Dr. S.H. Wilson	N/A
pGEX-2T-bPARG-GST	Dr. V. Schreiber	N/A
pXC53-hAPE1	Dr. S.H. Wilson	N/A
Software and Algorithms		
ImageJ 1.50i (Java 1.8.0_131 (32-bit))	Wayne Rasband, NIH, USA	https://imagej.nih.gov/ij/
GraphPad Prism	GraphPad Software, Inc	N/A
CellProfiler	Broad Institute, USA	https://cellprofiler.org/

CONTACT FOR REAGENT AND RESOURCE SHARING

Further information and requests for resources reagents should be directed to and will be fulfilled by the Lead Contact, David Pastré (david.pastre@univ-evry.fr).

EXPERIMENTAL MODEL AND SUBJECT DETAILS

Cell culture conditions

HeLa cells (female) were cultured in DMEM (Dulbecco's modified eagle's medium) supplemented with 10% FBS (fetal bovine serum) and penicillin-streptomycin (all GIBCO Life Technologies, United Kingdom). Cells were maintained at 37°C in a 5% CO_2 incubator. Cells were grown on 12 mm round coverslips inside 24-well plates for immunofluorescence or in Petri dishes (10 cm in diameter) for cell extract preparation.

Cell cultures, transfections and chemicals/drug treatment

Fresh culture medium with 5% serum was added to the cells before the transient transfections. HeLa cells were transfected with 1.5 μg of FUS-GFP encoding plasmid for each well by using Lipofectamine 2000. The cells were analyzed 24 h after plasmid DNA transfection. The efficiency of transfection was controlled by immunofluorescence or immunoblotting experiments (Figure S5a).

For oxidative stress induction, HeLa cells were treated with 300 μM hydrogen peroxide (H_2O_2) and incubated at 37°C for 15, 30 and 90 min. When indicated, cells were pre-treated with 10 μM olaparib for 15 min at 37°C or 5 μg/mL actinomycin D (ActD) at 37°C for 30 min before H_2O_2 treatment. After incubation with the drugs at indicated time-points or concentrations, the cells were washed with PBS and with 4% paraformaldehyde (PFA) in PBS for 45 min at 37 °C.

RNA interference

For the silencing of PARG or PARP-1, HeLa cells were then transfected with 20 nM of small-interfering RNA (siRNA) duplex using Lipofectamine 2000. A non-targeting sequence siRNA (AllStars Negative Control siRNA) was used as negative control. Cells transfected with the siRNA were placed in incubator at 37°C for 48 h, then the medium was replaced with fresh medium with 10% FBS, and cells were incubated for 24 h at 37°C. PARG or PARP-1 expression levels were analyzed by immunoblot 72 h after transfection using primary antibody.

METHODS DETAILS

Protein production and purification

The recombinant His-tagged PARP-1, APE-1 and GST-tagged PARG were overexpressed in *E. coli* strain BL21(DE3) pLysS and purified, as previously described (Amé et al., 2017; Sukhanova et al., 2004). The recombinant FUS, FUSΔLCD, FUSΔRGG1, FUSΔRGG1-2, FUS-6E, FUS-12E, HuR, G3BP1 or TDP-43 were overexpressed in *E. coli* strain BL21 (DE3) and purified as described below. Mutations for FUS-6E, S26E, S30E, T68E, S84E, S87E, S117E, and; FUS-12E, T7E, T11E, T19E, S26E, S30E, S42E, S61E, T68E, S84E, S87E, S117E S131E (Monahan et al., 2017).

Expression and purification of FUS, FUSΔLCD, TDP-43, HuR, G3BP1, FUS-6E, FUS-12E, FUSΔRGG1 or FUSΔRGG1-2

BL21(DE3) E.coli cells carrying plasmid pET-FUS, pET-FUSΔLCD, pET- FUS_1-374, pET- FUS_1-454, pET-MBP-FUS_FL_6E, pET-MBP-FUS_FL_12E, pET-TDP-43, pET-HuR or pET-G3BP1 were grown at 37°C in 2YT-ampicillin medium (1 L culture). When the optical density of the culture reached 0.7 OD at 600 nm, IPTG was added to a final concentration of 1mM, and growth was continued for 3 h. Cells were harvested and washed with 20 mL of cold buffer A containing 25 mM potassium phosphate, pH 7.4, 0.5 mM DTT,

1 mM PMSF and 1 M NaCl. The cell pellet (4 g wet) was suspended in 10 mL of the buffer A, and cells were disrupted by sonication in the cold (Bioblock Vibracell sonicator, model 72412). The resulting suspension was centrifuged at 4°C for 30 min at 150,000 x g in a TL100 Beckman centrifuge. In the case of G3BP1 protein, the supernatant was stored at −20°C and used for purification experiments. However, for FUS, FUSΔLCD, FUSΔRGG1, FUSΔRGG1-2, FUS mutants mimicking 6 or 12 phosphorylations (FUS-6E and FUS-12E), TDP-43 and HuR, the pellet was resuspended in 10 mL of the buffer A containing 6 M Urea and incubated for 120 min at 4°C. The resulting suspension was centrifuged at 4°C for 30 min at 200,000 x g in a TL100 Beckman centrifuge. The supernatant was stored at −20°C and used for purification experiments.

The His6-tagged proteins were purified as follows: soluble fractions described above were incubated for 2 h at 4°C with Ni^{2+}-NTA-agarose (15 mg of proteins/mL of resin) pre-equilibrated in buffer A. After incubation, the resin was transferred to an Econo-Pac chromatography column (Bio-Rad). The resin was then washed extensively with buffer A containing 20 mM imidazole and elution of the protein was obtained by increasing step by step the concentration of imidazole, from 40 to 250 mM, in buffer A. The purity of the resulting protein preparations was monitored at all stages of the purification by SDS-PAGE (Laemmli, 1970). The pure protein-containing fractions (100-250 mM imidazole) were concentrated to 2 mL and then dialyzed overnight against 100 volumes of buffer B (20 mM Tris-HCl, pH 7.4, 0.5 mM DTT, 6M urea and 200 mM NaCl). The final preparations were stored at −20°C.

In the case of FUS mutants mimicking 6 or 12 phosphorylations (FUS-6E and FUS-12E (Monahan et al., 2017), recombinant His_6-MBP-FUS-6 or His_6-MBP-FUS-12 was expressed in BL21(DE3) E.coli and purified as described above. His_6-MBP tag was cleaved off using a His_6-tagged TEV protease. Briefly, 1 mg of the protein was incubated with His_6-tagged TEV protease (10 μg) in buffer containing 25 mM Tris-HCl, pH 7.4, 1 mM DTT, 150 mM NaCl and 0.5 mM EDTA at room temperature for 20 h. SDS-PAGE was used to checked this proteolysis step. After that, EDTA was removed by using PD-10 Desalting column. Finally, the FUS-6E and FUS-12E proteins were separated from His6-tagged TEV protease and His6-MBP tag by using Ni^{2+}-NTA-agarose.

The purity of the proteins and proteolysis step were monitored at all stages of the purification by SDS-PAGE (Laemmli, 1970).

Preparation of DNA Substrates, mRNA and PAR

The 1200-bp nicked DNA containing a single nick in the middle of the chain was prepared as described previously (Sukhanova et al., 2016). The pBR322 (pBR) plasmid (or pT7) containing DNA breaks (damaged plasmid DNA) was prepared using heat and acid treatment to create abasic sites followed by AP site cleavage with apurinic/apyrimidinic endonuclease 1 (APE-1) activity. Briefly, plasmid DNA (0.25 mg/mL) was incubated in buffer containing 20 mM sodium citrate, pH 5.0 and 200 mM NaCl at 70°C for 4 hours. To induce single-strand breaks, the AP-site containing pBR (or pT7) plasmid (0.160 mg/mL) was incubated with 30 nM APE-1 in buffer containing 50 mM Tris-HCl, pH 8.0, 40 mM NaCl, 5 mM MgCl, 1 mM DTT for 1 h at 37°C. The DNA was rapidly chilled on ice and used for analysis.

To create linear plasmid DNA with blunt-ends the plasmids were linearized with enzymes EcoRV for pBR and Sma1 for pT7.

Linearized plasmid pSP72−2Luc, containing two full-length cDNAs of luciferases from *Renilla reinformis* and *Photinus pyralis* separated by a polylinker, was used as a template for RNA synthesis by T7 polymerase of 2Luc mRNA (~3000 nt). Transcription *in vitro* was performed by a HiScribe T7 High Yield RNA Synthesis Kit (New England BioLabs). Synthesized RNA was purified using phenol extraction.

PAR polymer was synthesized as described early (Amé et al., 2017). PAR yield was measured using the absorbance at 260 nm and the extinction coefficient of 13.5 $mM^{-1}cm^{-1}$ for ADP-ribose.

Preparation of samples for atomic force microscopy

Protein complexes for AFM analysis were formed in reaction mixtures (20 μL) containing binding buffer (12.5 mM HEPES, pH 7.6, 12.5 mM NaCl, 1 mM DTT, 100 mM urea), 3 nM PARP-1 and 40 nM of RNA-binding proteins and 1.25 nM 1200-bp nicked DNA, 2 nM 2luc mRNA or 1 μM PAR. To analyze the binding of proteins to mRNA in the presence of PAR, 40 nM FUS, FUSΔLCD, HuR or G3PB1 was pre-incubated with 2 nM mRNA and then the reaction mixtures were supplemented with PAR to a final concentration of 1 μM and further incubated for 30 s at 37°C.

To image protein complexes in the presence of auto-PARylated PARP-1, 30 nM PARP-1 was incubated with 12.5 nM 1200-bp nicked DNA, 12,5 nM supercoiled pBR and/or damaged pBR in the binding buffer containing 10 mM $MgCl_2$ and 0.3 mM NAD^+ at 37°C for 5 min. After that, the reaction mixtures were diluted 10-fold in the binding buffer containing 200 mM urea and incubated with 40 nM of RNA-binding proteins at 37°C for 1 min and immediately deposited on mica.

To analyze the dissociation of FUS/PAR compartments in the presence of PARG, the diluted reaction mixtures were pre-incubated with 40 nM FUS at 37°C for 1 min in the reaction buffer, followed by incubation with 4 nM PARG at 37°C and immediately deposited on mica.

To adsorb the molecules on mica, putrescine (Pu^{2+}) was added to the solution to a final concentration of 1 mM, after which a 10 μL droplet was deposited on the surface of freshly cleaved mica at room temperature for 30 s and dried for AFM imaging as describe previously.

AFM imaging and image analysis

AFM images were recorded in air by using a Nanoscope V Multimode 8 (Bruker, Santa Barbara, CA) in PeakForce Tapping (PFT) mode using Scanasyst-Air probes (Bruker). Continuous force-distance curves were thus recorded with an amplitude of

100-300 nm at low frequency (1-2 kHz). PFT mode decreases the lateral and shear forces. Images were recorded at 2048 × 2048 pixels at a line rate of 1.5 Hz.

Radioactive assay of protein PARylation and PAR hydrolysis by PARG *in vitro*

[^{32}P]-NAD$^+$ labeled on the adenylate phosphate was synthesized in a reaction mixture (100μL) containing 2 mM β-Nicotinamide mononucleotide, 1 mM ATP and 0.25 mCi of [α-^{32}P]-ATP (1000 Ci/mmol), 1.5 mg/mL nicotinamide mononucleotide adenylyl transferase (NMNAT), 25 mM Tris- HCl (pH 7.5), and 20 mM $MgCl_2$ was incubated for 1 h at 37°C. The enzyme was denatured at 65°C for 10 min and precipitated proteins were removed by centrifugation.

An *in vitro* poly(ADP-ribosyl)ation assay was performed in the reaction mixtures (20 μL) contained 20 mM Tris-HCl, pH 7.5, 25 mM NaCl, 1 mM DTT, 5 mM $MgCl_2$, 400 mM Urea, 0.05 A260/mL of DNase I-activated calf thymus DNA, 50 nM PARP-1, 0.3 mM NAD$^+$, 0.4 μCi [^{32}P]-NAD$^+$ and 2 μg FUS, FUSΔLCD, G3BP1, HuR, TDP-43, or BSA as indicated at the figure legends. The reactions were initiated by the addition of NAD$^+$. The reaction mixtures were incubated at 37 for 30 min and stopped by adding SDS-sample buffer and heating for 5 min at 90°C. The reaction mixtures were analyzed by 10% SDS-PAGE with subsequent phosphorimaging and/or colloidal Coomassie staining.

For the analysis of the degradation of PARP-1-bound PAR by PARG, 30 nM PARP-1 was incubated with 3 nM damaged pBR in the buffer containing 12.5 mM HEPES-KOH, pH 8.0, 25 mM NaCl, 1 mM DTT, 5 mM $MgCl_2$, 260 mM Urea, 400 μM, 0.3 mM NAD$^+$, 0.4 μCi [^{32}P]-NAD$^+$ at 37°C for 30 min followed by addition of EDTA to the final concentration of 15 mM. After that, the samples were supplemented with 2.4 μM FUS, FUSΔLCD, G3BP1, HuR or TDP-43 and incubated at 37°C for 5 min, and then PARG was added to final concentration 4 nM followed by incubation for 1-5 min at 37°C. The reaction mixture (20 μL) was stopped by adding 4 μL of the loading solution containing 90% formamide, 50 mM EDTA, 0.1% xylene cyanol, and 0.1% bromophenol blue, heated for 5 min at 95°C, and the products were separated by denaturing electrophoresis in 20% polyacrylamide gel followed by visualization with phosphorimaging.

Analysis of binding of FUS to RNA by EMSA

To assay stability of RNA-protein complexes in the presence of PAR, the reactions were performed in a mixture 25 μL containing 12.5 mM HEPES, pH 8.0, 25 mM KCl, 260 mM urea, 0.8 nM mRNA, 30-120 nM FUS and 0.4-4 μM PAR, as indicated in the figure legends. The reaction mixtures were incubated at 37°C for 10 min. Loading buffer (0.2 volume) containing 12,5 mM HEPES, pH 8.0, 50% glycerol and 0.015% bromophenol blue was then added to the samples. The RNA-protein complexes were analyzed by electrophoresis in 0.8% agarose in 0.5 X TBE buffer at room temperature at 5 V/cm followed by staining with SYBR Green II.

Co-sedimentation assays to probe the enrichment of damaged DNA in FUS/PAR compartments

A mixture (40 μL) containing 12.5 mM HEPES, 25 mM NaCl, 260 mM Urea, 5 mM $MgCl_2$, 1 nM linearized plasmid DNA (damaged or undamaged pBR/pT7), 10 nM PARP-1 and when indicated 0.3 mM NAD$^+$ was first prepared and incubated at 37°C for 5 min. After that the reactions were incubated with RNA-binding proteins (1 μM) for 5 min at 37°C. For sedimentation analysis, the reactions were centrifuged at 10,000 × g for 5 min at 25°C. Supernatants were collected, and pellets were resuspended in 20 μL of the buffer with 0.25 volume of the loading solution containing 5% SDS, 5% 2-mercaptoethanol, 0.3 M Tris-HCl (pH 6.8), 50% glycerol, and 0.015% bromophenol blue. Supernatants and pellets were divided into two parts. One part (20 μL) was analyzed by separation in 10% SDS-PAGE and visualized with Coomassie staining. The other part (20 μL) was resolved in a 0.8% agarose gel in 0.5 × TAE buffer at room temperature at 5 V/cm and stained with GelRed.

Immunofluorescence analysis

Cells were washed with PBS and fixed with 4% paraformaldehyde (PFA) in PBS for 45 min at 37 °C. After washing with PBS, coverslips were kept with blocking buffer (50 mM Tris pH 7.5, 100 mM NaCl, BSA 2%, 0.15% Triton X-100) for 40 min at 37 °C in order to permeabilize the cells and reduce nonspecific recognition by antibodies. Blocking buffer was removed and cells were washed and then incubated for 1 h at room temperature with primary antibody described in supplementary methods. The cells were washed 5 times with PBS and incubated for 1 h with fluorochrome (Alexa Fluor®488 and −594)-coupled secondary antibodies in 50 mM Tris pH 7.5. After final washes with PBS, the cells were stained with 300 nM DAPI to visualize the nuclei and mounted for fluorescence microscopy analysis.

Western blot analysis of PARG expression

Cells were lysed in 50 mM Tris-HCl, pH 7.5, 150 mM NaCl, 0.1% Triton X-100, 1 mm EDTA, and protease inhibitor mixture. Lysates were centrifuged at 14,000 × g for 15 min at 4°C, and supernatants were collected. Proteins (120 μg) of cell extracts were separated on 12% SDS-PAGE gels and transferred onto a PVDF membrane. The membranes were blocked in 5% (w/v) non fat dried milk, PBS for 30 min at room temperature (20°C) and incubated for 1 h at room temperature with primary anti-PARG and anti-tubulin antibodies. After that, membrane was washed in PBS 3 times for 5 min. Bound antibodies were detected and quantified using anti-mouse-IRDye 680 secondary antibodies with an Odyssey imaging system.

QUANTIFICATION AND STATISTICAL ANALYSIS

AFM analysis: images shown in the figures are representative of three different and independent samples. The ''particle analysis'' tool in the Nanoscope Analysis software (version 1.50) was used to determine the heights of the adsorbed molecules, PAR, RNA and multicomponent complexe particles from at least three independent samples. Basically, for each particles of interest, the particle analysis tool measured the maximum height of the particle. Significance of height were tested by using t test; *, $p < 0.05$; **, $p < 0.01$; ns, non-significant. The particle diameter is twice the smallest radius of a circle in which the particle can be placed.

Co-sedimentation analysis: quantification of the amounts of DNA in the pellets and supernatants was performed by measuring the integrated GelRed fluorescence intensity of a given band from agarose gels by using the Quantity One analysis software.

Analysis of cell by fluorescence microscopy: the measurements of the mean anti-FUS, anti-HuR, anti-TIA-1, anti-TDP-43, anti-SF1 or anti–PAR antibodies fluorescence intensities were performed using the ''CellProfiler'' software.